NASA TECHNICAL NOTE


NASA TN D-6664



NASA TN D-6664

# EXPERIMENTAL INVESTIGATION OF THE FLOW, OXIDATION, COOLING, AND THERMAL-FATIGUE CHARACTERISTICS OF A LAMINATED POROUS SHEET MATERIAL

*by Robert O. Hickel, Edward L. Warren, and Albert Kaufman*

*Lewis Research Center*
*Cleveland, Ohio 44135*

NATIONAL AERONAUTICS AND SPACE ADMINISTRATION • WASHINGTON, D. C. • FEBRUARY 1972

| 1. Report No. | 2. Government Accession No. | 3. Recipient's Catalog No. |
|---|---|---|
| NASA TN D-6664 | | |

4. Title and Subtitle: EXPERIMENTAL INVESTIGATION OF THE FLOW, OXIDATION, COOLING, AND THERMAL-FATIGUE CHARACTERISTICS OF A LAMINATED POROUS SHEET MATERIAL

5. Report Date: February 1972

6. Performing Organization Code:

7. Author(s): Robert O. Hickel, Edward L. Warren, and Albert Kaufman

8. Performing Organization Report No.: E-5872

10. Work Unit No.: 764-74

9. Performing Organization Name and Address:
Lewis Research Center
National Aeronautics and Space Administration
Cleveland, Ohio 44135

11. Contract or Grant No.:

13. Type of Report and Period Covered: Technical Note

12. Sponsoring Agency Name and Address:
National Aeronautics and Space Administration
Washington, D.C. 20546

14. Sponsoring Agency Code:

15. Supplementary Notes:

16. Abstract

The results of an experimental investigation made by the Detroit Diesel Allison Division of General Motors under two NASA contracts are summarized. The basic flow and oxidation characteristics of a laminated sheet-type porous material (Lamilloy) are presented. The oxidation characteristics of Lamilloy are compared to a wireform-type porous material for the case when both materials are made from Hastelloy-X alloy. The cooling performance of an air-cooled vane made from Lamilloy as determined from cascade tests made at gas temperatures ranging from 1388° to 1741° C (2350° to 3165° F) is presented. The results of a cascade-type thermal-fatigue test of the Lamilloy vane are discussed.

17. Key Words (Suggested by Author(s)):
Turbine cooling
Laminated porous sheet
Flow
Oxidation
Cooling
Thermal fatigue

18. Distribution Statement: Unclassified - unlimited

| 19. Security Classif. (of this report) | 20. Security Classif. (of this page) | 21. No. of Pages | 22. Price* |
|---|---|---|---|
| Unclassified | Unclassified | 51 | $3.00 |

* For sale by the National Technical Information Service, Springfield, Virginia 22151

# CONTENTS

# EXPERIMENTAL INVESTIGATION OF THE FLOW, OXIDATION, COOLING AND THERMAL-FATIGUE CHARACTERISTICS OF A LAMINATED POROUS SHEET MATERIAL

by Robert O. Hickel, Edward L. Warren, and Albert Kaufman

Lewis Research Center

## SUMMARY

Under two NASA contracts with the Detroit Diesel Allison Division of General Motors, experimental investigations of a laminated porous sheet material (having the trade name "Lamilloy") were made. The fluid flow and oxidation characteristics of the material were obtained using flow specimens. The oxidation characteristics of a wire-form porous material were also obtained and compared to Lamilloy. Both porous materials were made from Hastelloy-X. Air-cooled Lamilloy vanes were tested for their heat-transfer and thermal-fatigue performance in a five-vane static cascade facility. The cascade tests were made at gas temperatures up to about $1741^{\circ}$ C ($3165^{\circ}$ F).

The internal flow characteristics of Lamilloy were correlated by using equations previously developed for wireform and sintered powdered-metal types of porous materials. Lamilloy exposed to an oxidizing atmosphere was found to be significantly less sensitive to internal flow reductions than was the wire-wound porous material exposed to the same atmosphere. Experimental investigation of Lamilloy vanes in a cascade indicated that the leading-edge region consistently operated hotter than any other region of the airfoil. The average vane wall temperature difference ratio (total gas temperature minus the average vane wall temperature divided by the total gas temperature minus the coolant inlet temperature) was approximately constant at values of about 0.6 to 0.7 over the range of test conditions investigated. Predicted airfoil temperatures were calculated for the vanes: the comparison between predicted and experimental temperatures ranged from good to poor: the general trends of the temperatures, however, were predicted fairly well.

A group of test vanes installed in the cascade and subjected to 3-minute cycles wherein the gas temperature was rapidly changed from $617^{\circ}$ to $1537^{\circ}$ C ($1140^{\circ}$ to $2800^{\circ}$ F) were found to have leading-edge cracks when first inspected after 110 cycles. Chordwise cracks in all test vanes were caused by thermal fatigue as a result of large chordwise temperature gradients in the airfoils. A large radial crack in one vane was caused by the cold forming process used in the fabrication of the airfoils. A thermal-fatigue analysis, applied to the vanes for the operating conditions observed during the tests, predicted failure of the vanes between 142 and 260 thermal cycles.

# INTRODUCTION

Under two NASA contracts, the Detroit Diesel Allison Division of the General Motors Corporation investigated a sheet-type porous material for possible application to transpiration-cooled turbine vanes. The porous material investigated consisted of laminated, photoetched metal sheets which form a porous medium known as "Lamilloy" (ref. 1). Lamilloy is a registered trademark of the Detroit Diesel Allison Division of the General Motors Corporation. The results of these contract investigations were published in three reports (refs. 2 to 4). The purpose of this report is to summarize the results of references 2 to 4.

In reference 2 the basic flow characteristics were determined for 15 different internal geometries of Lamilloy. In addition, the oxidation and strength characteristics of Lamilloy were compared to a wire-wound porous material. Both the Lamilloy and the wire-wound porous material were made from Hastelloy-X.

In reference 3 the design and experimental cooling performance of a vane made from Lamilloy are discussed. The vane was investigated in a five-vane cascade at nominal combustion gas temperatures that ranged from $1093^{\circ}$ to $1741^{\circ}$ C ($2000^{\circ}$ to $3165^{\circ}$ F) at a gas stream pressure level of 78.7 $N/cm^2$ (114 psia) and with a cooling air inlet temperature to the vanes that ranged from $316^{\circ}$ to $454^{\circ}$ C ($600^{\circ}$ to $850^{\circ}$ F). One test was made at a gas pressure of 96.5 $N/cm^2$ (140 psia) and a nominal gas temperature of $1371^{\circ}$ C ($2500^{\circ}$ F).

The International System of Units is used throughout this report as the primary system. United States customary units are included in parentheses; calculations were performed in the United States customary units.

Reference 4 presents the results of a thermal-fatigue investigation of three Lamilloy vanes installed in a static cascade. The vanes were subjected to thermal cycling by varying the combustion gas temperature of the cascade from nominal values of $621^{\circ}$ C ($1150^{\circ}$ F) to $1538^{\circ}$ C ($2800^{\circ}$ F) and back to $621^{\circ}$ C ($1150^{\circ}$ F). Each nominal gas temperature level was maintained for 90 seconds. In order to subject the porous walls of each vane to a different thermal response, the cooling air temperature during the cycle was different for each vane, ranging from a low of about $271^{\circ}$ C ($520^{\circ}$ F) to a high of about $516^{\circ}$ C ($960^{\circ}$ F).

Since the main purpose of this report is to summarize the results of references 2 to 4, only a necessary minimum of procedure and apparatus is reported herein; these aspects of the program are discussed in detail in references 2 to 4.

It should be noted that throughout the present report some of the written material in references 2 to 4 has been incorporated herein verbatim.

# DESCRIPTION OF POROUS MATERIALS

This investigation deals primarily with the laminated porous sheet material produced by the Allison Division under the trade name Lamilloy. The oxidation characteristics of Lamilloy are compared to those of a wire-wound porous material. A description of each of the materials is given in this section.

## Lamilloy

Isometric sketches of typical sheets of Lamilloy are shown in figures 1(a) and (b). Lamilloy consists of three (or five) thin sheets that are bonded together. Two of the sheets have a grid pattern; sheets with a "standard" circular pedestal grid pattern are shown in figure 1(a), while a "connected" grid pattern is shown in figure 1(b). The third sheet of the three-layer laminate has no grid. Each of the sheets has an array of holes which permit the flow of air from one sheet to the adjacent sheet. By adjusting the size of the holes, the spacing of the holes, the geometry of the grid, the depth of the grid, and the number of laminates, the airflow through the Lamilloy sheet can be controlled for a given pressure drop across the laminates.

In order to determine the effect of the internal geometry of Lamilloy on the permeability (relationship between airflow and pressure drop), a series of 15 different internal flow configurations of Lamilloy were investigated. Fourteen configurations had grid arrays consisting of circular lands as shown in figure 1(a); one had "connected" arrays as shown in figure 1(b). One configuration had five laminates; all others had three laminates. In the case of the five-laminate configuration, four sheets had pedestal grid patterns and one outer sheet had no grid. Table I summarizes the geometric parameters investigated; for convenience, the variables and their associated nominal ranges are listed here (the various geometry factors are defined in fig. 1):

| | |
|---|---|
| Grid depth, cm (in.) | 0.0024 to 0.0117 (0.00095 to 0.0046) |
| Hole diameter, cm (in.) | 0.036 to 0.064 (0.014 to 0.025) |
| Hole spacing, cm (in.) | 0.122 to 0.366 (0.048 to 0.144) |
| Overall thickness, cm (in.) | 0.033 to 0.1029 (0.013 to 0.0405) |
| Laminate thickness, cm (in.) | 0.010 to 0.033 (0.004 to 0.013) |
| Number of laminates | 3 and 5 |
| Grid spacing, cm (in.) | 0.033 and 0.061 (0.013 and 0.024) |
| Grid types | Standard and connected |
| Pedestal diameter, cm (in.) | 0.036 and 0.066 (0.014 and 0.026) |

The selection of the configurations was based on considerations such as permeability level desired, strength, and ease of fabrication. The 15 configurations selected were believed to provide a range of flow geometries that would supply basic information relative to permeability and oxidation characteristics that would be applicable to the eventual design of vanes for operation in a static cascade.

## Wire-Wound Porous Material

Hereinafter the wire-wound porous material shall be identified as "WPM." WPM is fabricated by systematically winding flattened wire around a cylindrical mandrel. It is then placed in a dry hydrogen-atmosphere furnace at elevated temperature; this results in sintered bonds between contacting wires. After sintering, the mandrel is removed and the resulting cylindrical tube is cut and rolled into sheets of WPM of the desired thickness and permeability. The internal structure is ordered and provides small passages for the flow of air. Figure 2 is an isometric sketch of a section of WPM. The permeability of WPM is a function of overall thickness, wire size, wind angle, and wire spacing. Additional information about the basic construction techniques and characteristics of a typical wire-wound porous material is given in reference 5.

For this investigation, the Lamilloy and WPM were made of Hastelloy-X. This is a high-temperature nickel-base alloy and was selected because of its good high-temperature properties (ref. 6) and its ready availability in both sheet and wire form. Hastelloy-X also exhibits good stress-rupture and ductility characteristics in the 760° to 982° C (1200° to 1800° F) temperature range.

# TEST SPECIMENS AND VANES

## Flow Test Specimens

The basic flow characteristics of Lamilloy and the effects of oxidation on the flow characteristics of Lamilloy and WPM were obtained with disk-type specimens having a diameter of 2.873 centimeters (1.132 in.). Typical Lamilloy and WPM disk specimens are shown in figure 3.

## Cascade Test Vanes

A cross section of the vane airfoil is shown in figure 4(a). A cross section of the porous shell before it is formed into an airfoil is shown in figure 4(b). The design incorporates a Lamilloy shell having three different permeability levels as indicated in figure 5. The resistance coefficients and flow rate parameter shown in figure 5 are discussed later in the section RESULTS AND DISCUSSION. Symbols are defined in the appendix. The portion of the Lamilloy shell which actually metered the airflow through the wall was about 0.0762 centimeter (0.030 in.) thick and consisted of layers 4 to 6 as shown in figure 4(a). These layers were reinforced by stiffening sheets (layers 1 to 3) to provide structural rigidity to the bonded assembly. Oversized holes, having a diameter of 0.112 centimeter (0.044 in.), were photoetched in the stiffening sheets to connect the airfoil central core (coolant supply plenum) to the metering sheets. The holes in the stiffening sheets and in layer 4 of the metering sheets were concentric. The overall thickness of the metering sheets and stiffening sheets was 0.191 centimeter (0.075 in.).

The composite wall structure was first fabricated in flat sheet form and then cold formed into the airfoil shape. After forming, the trailing-edge region of each side wall was joined by welding. The completed airfoil had a span of about 10.2 centimeter (4 in.) and a chord of about 5.7 centimeters (2.2 in.).

End attachments were provided to facilitate assembly of the vanes in the cascade facility. A cooling air duct was incorporated in the outer-radius end-attachment to permit delivery of coolant to the vane. A view of the pressure and suction sides of a typical, fully assembled vane is shown in figure 6. The Lamilloy vane was designed to operate at the following conditions:

(1) Average total gas temperature into the cascade vane row, 1371° C (2500° F)

(2) Cooling air temperature at the vane inlet, 649° C (1200° F)

(3) Gas stream inlet total pressure, 78.6 $N/cm^2$ (114 psia)

(4) The external aerodynamic configuration and aerodynamic conditions shown in reference 7

(5) A cooling air flow rate necessary to maintain a nominal skin temperature of 871° C (1600° F)

The design metal temperature of 871° C (1600° F) was selected to provide an acceptable oxidation life of the airfoil material, as is discussed in the section Vane Design. Three different nominal permeability levels were selected for the airfoil wall and were distributed around the airfoil as indicated in figure 5.

# APPARATUS

## Permeability Test Equipment

The ambient-temperature flow facility for determining the flow characteristics of disk-type Lamilloy and WPM specimens is shown in figure 7. Figure 7(a) shows the equipment; figure 7(b) is a schematic diagram of the flow and measurement systems. Air was supplied at 87.7 $N/cm^2$ (120 psig). Pressure reduction and flow control were achieved with a manually controlled pressure regulator and valve. The pressures upstream and downstream of the test specimen were measured with manometers and pressure gages. The flow rate was measured using a gas meter and a stopwatch. A similar facility, incorporating an electric air heater, was used to obtain the flow characteristics of disk-type specimens at an air temperature of $150^{\circ}$ C ($300^{\circ}$ F) at the test specimen.

## Cascade Facility

The vanes were investigated in a simulated engine environment in a high-temperature cascade facility shown schematically in figure 8. This is a variable-geometry cascade and is capable of testing various blade and vane sizes with minimum system modification. For this investigation, the cascade combustion gas flow was varied from about 4.53 to 6.1 kilograms per second (10 to 13.5 lb/sec), pressures were 78.6 and 96.5 $N/cm^2$ (114 and 140 psia), and nominal gas total temperature ranged from about $1093^{\circ}$ to $1741^{\circ}$ C ($2000^{\circ}$ to $3165^{\circ}$ F).

Five vanes were used in each cascade test. Figure 9 shows a view (looking downstream into the cascade entrance) of five vanes mounted in the cascade test fixture. In the cooling performance tests, the center vane was the test vane and the others were slave vanes. For identification purposes, the vane positions were numbered as shown in figure 9. For the thermal-fatigue tests, vanes in positions 2 to 4 were the test vanes.

Four sight ports looking directly at vane 3 are shown in figures 8(a) and (b). The surface temperature of the vane airfoils was obtained optically through the sight ports.

## Cascade Instrumentation

A summary of the cascade instrumentation is given in the following paragraphs:

Flow rates. - Cooling air and combustion air flow rates were determined by the use of thin plate orifices. The fuel flow rate to the combustor was measured with a turbine-type flowmeter. The combustion gas flow rate to the vane test section was then the sum of the combustion air flow rate and the fuel flow rate.

Gas pressure. - The combustion gas static pressure was measured with two static pressure taps on the transition section inner wall about 3.18 centimeters (1.25 in.) upstream of the vanes. The average gas total pressure was then computed.

Gas temperature. - The combustion gas temperature was determined by using nonshielded platinum/platinum-rhodium thermocouples. The gas passage immediately upstream of the vanes was traversed thoroughly to obtain an average gas temperature. The gas temperature thermocouple locations for various probes are shown in figure 10.

Cooling air pressure and temperature. - A static-pressure probe and a thermocouple were mounted in each vane cavity to measure cooling air inlet conditions.

## Vane Instrumentation

Heat-transfer tests. - The vane wall temperatures (surface temperature) were obtained with an infrared photographic pyrometry system. The test vane surfaces were photographed through the cascade sight ports discussed previously. The photographic images were recorded on film sensitive to infrared radiation. The density of the developed film was related to the vane surface temperature by calibration of the system. The system and the calibration method are discussed in detail in references 3 and 8.

Thermal-fatigue tests. - Thermocouples, as well as infrared photographs, were used to measure the airfoil metal temperatures in the thermal-fatigue tests. Six thermocouples were installed on each of vanes 2, 3, and 4 at a depth of approximately 0.127 millimeter (0.005 in.) beneath the outer surface of the airfoil. The thermocouples were located so that at least two could be viewed through each sight port. These thermocouples served as a basis for relating the infrared photographic data (film density) to a known temperature. The infrared photographic procedure is discussed in references 4 and 8.

# EXPERIMENTAL PROCEDURE

## Basic Permeability Investigation

Disk-type specimens were used to determine the basic pressure drop - flow relationship for the Lamilloy and WPM materials. The specimens were tested in the ambient flow facility and/or the 150° C (300° F) flow facility described previously. Data were obtained over a range of pressure drops for each specimen. The pressure drop was varied from zero to about 69.0 N/cm$^2$ (100 psia). The discharge side pressure was 1 atmosphere.

## Oxidation Investigation

In order to determine the effects of oxidation on the flow characteristics of Lamilloy and WPM, a total of 24 disk-type specimens (12 of Lamilloy and 12 of WPM) were selected for exposure to elevated temperature in electric furnaces. The Lamilloy specimens were selected so that they all had similar initial permeabilities. The WPM specimens had initial permeabilities equal to or greater than the Lamilloy specimens. After initial flow testing, the specimens were divided into four groups; each group consisted of three Lamilloy and three WPM specimens. The first group was used exclusively for oxidation exposure at a temperature of $760^{\circ}$ C ($1400^{\circ}$ F), the second group for exposure at $871^{\circ}$ C ($1600^{\circ}$ F), the third group for exposure at $983^{\circ}$ C ($1800^{\circ}$ F), and the fourth group for exposure at $1093^{\circ}$ C ($2000^{\circ}$ F). Each group was heated for 4 hours in a still atmosphere at its respective temperature level. Then each specimen was removed from the furnace and flow tested at room temperature. The same procedure of heating and flow testing was repeated after accumulated furnace exposure times of 12, 60, 100, 200, 300, 400, 500, and 600 hours.

## Vane Cooling Performance Investigation

The investigation of the cooling performance of Lamilloy vanes was conducted in the static cascade facility described previously. The tests were made at the nominal conditions specified in table II. The pressure ratio across the vane row was adjusted so a constant corrected flow $W_g\sqrt{\theta}/\delta$ of 1.45 kilograms per second (3.2 lb/sec) was maintained at the throat of the airfoils. This was done to assure that the local surface velocity distributions would be about the same as those on which the vane thermal design was based. The details of procedures for operating the cascade and setting test points are given in reference 3. The methods used for correcting the observed gas temperatures for radiation and the vane surface temperatures for gas luminosity are also given in reference 3.

## Thermal-Fatigue Investigation

Five vanes that had not been previously exposed to elevated temperatures were installed in the static cascade for investigation of their thermal-fatigue characteristics. The vanes were subjected to repeated thermal cycling by varying the combustion gas temperature from nominal values of about $617^{\circ}$ to $1537^{\circ}$ C ($1140^{\circ}$ to $2800^{\circ}$ F) and back to $617^{\circ}$ C ($1140^{\circ}$ F). Each nominal gas temperature level was maintained for 90 seconds, and the changes in gas temperature were accomplished in about 1.8 seconds. The

temperature of the cooling air (at the entrance to the vane cavity) was different for each of the test vanes as indicated in the following table:

| Test vane | Cooling air temperature at inlet to vane cavity | | | |
|---|---|---|---|---|
| | Low gas temperature | | High gas temperature | |
| | $^{o}C$ | $^{o}F$ | $^{o}C$ | $^{o}F$ |
| Vane 2 | 271 | 520 | 332 | 630 |
| Vane 3 | 432 | 810 | 368 | 695 |
| Vane 4 | 417 | 782 | 516 | 960 |

At the start of the thermal-fatigue tests, the cascade combustion gas conditions were set to obtain an average combustion gas inlet temperature of about 1538° C (2800° F) and a corrected gas flow rate $W_g\sqrt{\theta}/\delta$ of 1.45 kilograms per second (3.2 lb/sec) per vane channel. The coolant flow to each of the test vanes was individually adjusted so that the maximum wall temperature (as indicated by thermocouples) at the leading edge of each vane was about 937° C (1700° F).

When the desired nominal "low" and "high" gas temperature and associated operating conditions had been set, the cascade gas temperature conditions were then automatically cycled.

# RESULTS AND DISCUSSION

## Correlation of Experimental Flow - Pressure Drop Data

The pressure drop and flow data were correlated in terms of dimensionless parameters originally suggested by Green (ref. 9). The Green equation can be written as

$$\frac{(P_1^2 - P_2^2)g}{\tau\mu^2(2RT)} = \alpha\left(\frac{G}{\mu}\right) + \beta\left(\frac{G}{\mu}\right)^2 \tag{1}$$

The linear term of the quadratic represents the viscous shear contribution to the pressure drop, and the squared term represents the inertial contribution to the pressure drop. Two empirical constants, $\alpha$ and $\beta$, must be determined experimentally for a given porous matrix.

One of the objectives of the experimental flow program was to determine if the fluid pressure drop across Lamilloy could be correlated in the manner suggested by

equation (1) so that a given Lamilloy configuration could be characterized by the two empirical constants $\alpha$ and $\beta$. A simple graphical representation of equation (1) can be made by plotting $(P_1^2 - P_2^2)g/2\mu\tau RTG$ against $G/\mu$, which is equivalent to rewriting equation (1) as

$$\frac{(P_1^2 - P_2^2)g}{2\mu\tau RTG} = \alpha + \beta\left(\frac{G}{\mu}\right) \tag{2}$$

The slope of the plot then represents $\beta$ and the intercept represents $\alpha$.

The flow - pressure drop data taken with both ambient and 150° C (300° F) air were correlated in terms of equation (2). A typical result is shown in figure 11, which presents the ambient and high-temperature airflow test results for a relatively "high flow" permeability level of Lamilloy. Data for WPM of similar high permeability are shown for comparison. The results show that flow through Lamilloy is correlated well by Green's equation for both ambient and 150° C (300° F) air. Some more recent results reported in reference 10 show that equation (1) and the $\alpha$ and $\beta$ parameters determined at room temperature can predict the flow rate of 449° C (840° F) air through a Lamilloy wall.

A summary of the $\alpha$ and $\beta$ values for the 15 different Lamilloy configurations is given in table III. The table also lists the associated values of permeability-coefficient-to-thickness ratio, $K'/\tau$. By definition, $K'/\tau = (2RT\mu G_{10})/(P_1^2 - P_2^2)$, where $P_1$ is 17.0 N/cm$^2$ (24.7 psia), $P_2$ is 10.1 N/cm$^2$ (14.7 psi), and T is 24° C (75° F). The term $G_{10}$ is the specific flow rate at these standard conditions.

Equation (2) may be rewritten by dividing both sides by $\beta(G/\mu)$ so

$$\frac{(P_1^2 - P_2^2)g}{\beta RT\tau G^2} = 2\left[\left(\frac{\alpha\mu}{\beta G}\right) + 1\right] \tag{3}$$

Since the ratio $\beta/\alpha$ has units of length, a characteristic Reynolds number for the porous matrix may be defined as $Re = (G/\mu)(\beta/\alpha)$. By substituting for Re in equation (3), a flow resistance factor $C_f$ is obtained as the expression

$$C_f = \frac{(P_1^2 - P_2^2)g}{\beta RT\tau G^2} = \frac{2}{Re} + 2 \tag{4}$$

Equation (4) may be considered a universal resistance law for porous material in which all flow data, regardless of the specific porous configuration, should be correlated.

Therefore, all the data taken in the flow studies of all 15 Lamilloy configurations were plotted in figure 12 with the flow resistance factor $C_f$ as the ordinate and the Reynolds number $(G/\mu)(\beta/\alpha)$ as the abscissa. All the data correlated well, as expected, since equation (4) is merely a manipulation of equation (2).

The experimentally determined coefficients $\alpha$ and $\beta$ characterize the flow through a given Lamilloy configuration. In reference 10 the $\alpha$ and $\beta$ coefficients were correlated for the 13 standard grid arrays (table I) against matrix parameters which were combinations of the hydraulic diameter of the minimum internal constriction and the external hole spacing. Two grid arrays (configurations 10 and 11 of table I) did not correlate by the method of reference 10. Figure 13 is a reproduction from reference 10 showing the correlations of $\alpha$ and $\beta$, for the standard grid arrays, against their respective matrix parameter. With the use of figure 13, $\alpha$ and $\beta$ can be predicted for a given Lamilloy configuration with a standard grid array, when only the geometry is known.

## Effects of Oxidation on Flow Characteristics

The purpose of this phase of the investigation was to determine the effects of an oxidizing atmosphere on the flow characteristics of Lamilloy and WPM. Disk-type specimens were placed in ovens and heated to elevated temperatures ranging from $760^{\circ}$ to $1093^{\circ}$ C ($1400^{\circ}$ to $2000^{\circ}$ F) as discussed previously in the section EXPERIMENTAL PROCEDURE. The specimens were first flow tested, then heated for specified time intervals, and flow tested again. Because the permeability level of all specimens before exposure to the oxidizing environment was approximately the same, a direct comparison of the oxidation effects on Lamilloy and WPM made from Hastelloy-X material could be made. The true measure of the effect of oxidation on flow characteristics is reflected by the change in the $\alpha$ and $\beta$ values of the test specimens. These changes are presented in reference 2; and the $\alpha$ and $\beta$ values for each test specimen, as a function of time, are tabulated therein. By using each $\alpha$ and $\beta$ combination, a value of standard flow rate $G_{10}$ as a function of time was determined and is tabulated in reference 2. The average values of $G_{10}$ for the oxidation test specimens as a function of exposure time are plotted in figure 14, where the Lamilloy and WPM results are indicated by solid- and dashed-line curves, respectively.

It can be seen that there was a general trend for the flow to decrease with exposure time for both Lamilloy and WPM; furthermore, the decrease in flow rate was more rapid for the specimens subjected to the higher exposure temperatures. Also, the WPM showed significantly greater decreases in flow for a specific exposure temperature than did the Lamilloy. For example, after 600 hours exposure at $760^{\circ}$ C ($1400^{\circ}$ F), the Lamilloy flow was reduced about 5 percent, while that for WPM was reduced about 33 percent. At $871^{\circ}$ C ($1600^{\circ}$ F) and 600 hours, Lamilloy flow was reduced about 12 percent

and WPM about 82 percent. For 982° C (1800° F) exposure temperature, WPM exhibited a marked decrease in flow: after 100 hours of exposure, the flow was reduced about 92 percent; and a complete loss in permeability was noted after less than 400 hours. For the 982° C (1800° F) exposure, Lamilloy was reduced only about 13 percent after 200 hours and about 28 percent after 600 hours. Both materials exhibited very rapid reductions in flow after exposure to 1094° C (2000° F); WPM lost about 90 percent of its flow capability after 12 hours exposure and became completely clogged shortly thereafter. At the highest exposure temperature, Lamilloy lost about 94 percent of its flow capability after 400 hours exposure and was completely clogged after about 440 hours exposure.

In an actual transpiration cooling application, two factors are present that were not encountered in the investigation made herein: (1) air flows through the material during temperature exposure, and (2) the metal temperature is nonisothermal in the direction of airflow. Both of these factors may reduce the oxidation effects and thus make the results herein somewhat pessimistic for design purposes. It is believed, however, that the results obtained provide a realistic measure of the relative clogging due to oxidation for Lamilloy and WPM made from Hastelloy-X alloy.

It should be noted that Hastelloy-X material is probably not the most oxidation-resistant alloy from which Lamilloy or WPM can be made. Reference 11 shows that WPM made from GE 1541 material (an iron-chromium-aluminum-yttrium heating-element alloy) had no reduction in coolant flow after 600 hours of exposure at a temperature of 982° C (1800° F).

## Vane Design

After the basic flow and oxidation characteristics of Lamilloy were known, it was then possible to thermally and structurally design a vane for the cascade. For the thermal design it was ideally desired that the vane airfoil have an isothermal skin temperature of about 871° C (1600° F). This skin temperature level was selected based on the results of the previously discussed oxidation tests. Figure 14 indicates that for a Lamilloy skin temperature of 871° C (1600° F), the reduction in coolant flow due to oxidation would be less than 10 percent for exposures of the order of 300 hours. It was anticipated that the operating times of the vanes in the cascade would be much less than 300 hours and, therefore, clogging due to oxidation would be small for vane wall temperatures up to 871° C (1600° F).

As mentioned previously in the section TEST SPECIMENS AND VANES, the vane airfoil had three areas of different nominal permeability. The values of $\alpha$ and $\beta$ associated with each area are indicated in figure 5. The range of the value of the flow rate parameter $G/\mu$ is also tabulated in figure 5; the large variations in $G/\mu$ within a given

area of constant permeability are caused by the variations in static pressure of the gas stream around the vane.

## Effect of Cascade Tests on Vane Permeability

After the cascade cooling investigation was completed, the test airfoils were investigated for their local flow characteristics. The complete local flow data are given in reference 3. A typical example of the post-test flow results is given in figures 15(a) and (b) where the $\alpha$ and $\beta$ values, respectively, are shown for the midspan plane of one test vane. The symbols on the figure indicate post-cooling-test data; the data obtained prior to testing (on the individual airfoil blanks) are shown as dashed lines and represent average values over a given segment of the airfoil. The design permeability values are shown as solid lines. The viscous flow coefficient $\alpha$ increased during the cascade test period. The inertial resistance coefficient $\beta$ increased in the suction and leading-edge regions and decreased in the pressure surface region. For the flow regime or blowing rates of interest herein (see fig. 5), the $\beta$ factor has the greatest influence on the flow through the Lamilloy material, while the effect of $\alpha$ is of secondary importance. In general, the average values of $\alpha$ and $\beta$ increased during the testing period and thus reduced the flow through the vanes for a given pressure drop across the airfoil.

The post-test $\alpha$ and $\beta$ data shown in figure 15 resulted in the values of $G_{10}$ increasing (relative to the "before forming" values) about 2 percent for the pressure surface (area A of fig. 5). For the suction surface (area B) and the leading edge (area C), the $G_{10}$ values decreased about 10 and 51 percent, respectively. The decreases in flow were greater than those expected based on the specimen flow data of figure 14 and the vane wall temperatures observed during cascade operation. As is discussed in greater detail later in the section Experimental Evaluation of Vane Cooling Performance, the maximum airfoil wall temperatures occurred at the leading edge and were generally no greater than about $871^{\circ}$ C ($1600^{\circ}$ F). It should be noted that the "base" flow data before cascade operation were obtained from flat sheets of Lamilloy. Subsequent airfoil forming operations, particularly those associated with the relatively small-radius leading-edge region, may have significantly reduced the permeability.

## Experimental Evaluation of Vane Cooling Performance

Typical experimental airfoil metal temperature distributions are shown in figures 16 to 19 by the data points. Local metal surface temperature is shown as a function of the surface distance from the suction-side trailing edge. The data shown in figures 16 to 19 have been corrected to account for gas stream luminosity effects (the details of this

correction are given in appendix E of ref. 3). The solid-line curves represent predicted temperatures and are discussed later in the section Comparison of Experimental and Predicted Temperatures. The experimental data show that the peak airfoil surface temperature occurs at or near the airfoil leading edge. In general, the downstream suction surface temperatures are quite low (about $225^{\circ}$ C ($400^{\circ}$ F) lower than the leading edge, except in fig. 19 where the difference is only about $110^{\circ}$ C ($200^{\circ}$ F)). The suction surface temperatures increase near the trailing-edge region; this may be the result of insufficient cooling air reaching the extreme trailing-edge region of the central cooling air plenum chamber (see fig. 4). Surface temperatures along the pressure surface typically decreased from leading edge to trailing edge. Average airfoil surface temperatures were $83^{\circ}$ to $111^{\circ}$ C ($150^{\circ}$ to $200^{\circ}$ F) lower than peak values. The highest observed surface temperature shown herein was $882^{\circ}$ C ($1620^{\circ}$ F).

A common parameter, known as the temperature difference ratio or simply as $\varphi$, is often used in evaluating the performance of air-cooled vanes and blades. For vanes, $\varphi$ can be defined as $(T_T - T_w)/(T_T - T_c)$ where $T_T$, $T_w$, and $T_c$ are the gas total temperature, the airfoil surface temperature, and cooling air inlet temperature, respectively. Figure 20 presents the variation of the cooling performance parameter $\varphi$ as a function of the dimensionless ratio $W_c/W_g$ (coolant flow rate divided by gas flow rate). The average value of the vane midspan surface temperature was used to determine the value of $\varphi$ in figure 20, and data for all test runs are represented. It can be seen that $\varphi$ ranged in value from about 0.6 to 0.7 for the range of experimental data; furthermore, $\varphi$ was relatively insensitive to a change in coolant flow.

The insensitiveness of the average wall temperature to changes in the coolant flow may be caused by several factors. For coolant flow ratios of the order of 0.4 or more, the influence of the local blowing rate $G/\mu$ on reducing the heat flux from the gas into the vane wall probably becomes less effective as the coolant flow is increased. The higher coolant flow rates result in higher velocities leaving the Lamilloy, thus promoting mixing with the hot gas. Therefore, relatively small average wall temperature reductions may result from significant increases in coolant flow. Also, the changes in overall coolant flow rate may cause changes in the local distribution of coolant through the Lamilloy walls. The redistribution of coolant may not change the average wall temperature significantly as the coolant flow is increased; and, therefore, only a small change in the dimensionless temperature ratio parameter would result.

## Comparison of Experimental and Predicted Temperatures

The predicted temperature distributions shown in figures 16 to 19 were obtained by using the following experimental data as input to the calculation procedure:

(1) The measured radial gas temperature profile (the measured gas temperatures were corrected for recovery and radiation effects as discussed in appendix D of ref. 3)

(2) The measured gas stream and coolant supply pressures

(3) The measured coolant temperature into the vane

(4) The measured post-test permeability data

The metal temperature calculation procedure was based on the simultaneous solution of coupled boundary layer porous wall energy and momentum conservation equations presented in reference 3. The prediction of airfoil metal temperatures can be subdivided into five basic steps as follows:

(1) By using specified airfoil Mach number distributions (ref. 7) and the gas pressure and temperature conditions obtained experimentally, compute the local surface gas velocity, static pressure, and static temperature distributions using isentropic relationships.

(2) For the experimental values of coolant supply pressure and temperature, the measured permeability distribution, and the airfoil surface static-pressure distribution from step 1, calculate the local injection rates using equation (B6) of reference 3.

(3) Determine the airfoil skin temperature distribution by the simultaneous solution of equations (B1) and (B3) of reference 3.

(4) Using the injection rates determined in step 2 and the surface temperatures calculated in step 3, calculate the temperature distribution in the metering layers (layers 4 to 6 in fig. 4(a)) using equation (B16) of reference 3.

(5) Determine the temperature gradient across the stiffener portion of the vane wall (layers 1 to 3 in fig. 4(a)) by assuming that all the heat transferred to the interface of layers 3 and 4 passes through the stiffener sheets and is then absorbed by the coolant.

In reference 3, vane temperature predictions were made for five different cascade operating conditions and for three different spanwise planes on the test vane. Therefore, a total of 15 chordwise vane surface temperature predictions were made. Only four of the predicted temperature distributions are shown in this report to summarize the results presented in reference 3. The following comments apply to the general results that were obtained in reference 3 and usually apply to the specific results shown in figures 16 to 19.

The measured temperatures on the pressure side of the airfoil were generally higher than predicted. The temperature corrections made to the measured surface temperatures for gas luminosity effects (from $0^{\circ}$ to $33^{\circ}$ C ($0^{\circ}$ to $60^{\circ}$ F)) may have been too low (conservative). Reference 3 indicates that the gas luminosity effects were significant for the pressure-side region. The experimental data indicate that the correction method may underestimate the correction factors required.

The agreement between measured and predicted temperatures on the suction side was good in some cases and poor in others. The large differences between measured and predicted temperatures at a distance of about 1 to 4 centimeters (0.4 to 1.6 in.) from the trailing edge may have been caused, in part, by gas luminosity effects and, in part, by lack of accuracy in the calculated surface static-pressure and velocity distributions in this region.

It can be seen in figures 17 to 19 that a nearly constant temperature was predicted for the suction surface in a region extending from the trailing edge to about 0.5 to 1 centimeter (0.2 to 0.4 in.) from the suction-side trailing edge. This predicted temperature trend resulted from an assumption made in the prediction technique because the variation of permeability in the trailing edge was not known experimentally. It was not possible to accurately measure the local permeability in the extreme trailing-edge region because of the size of the permeability probe used. Therefore, in the prediction calculations, the permeability was assumed to be constant and equal to the experimental permeability values measured closest to the trailing edge. This assumption may have been inaccurate and led to optimistically low values of predicted temperature.

For the leading-edge region of the vane (about 0.76 cm (0.3 in.)) along the pressure and suction surface from the stagnation point), the agreement between the predicted and measured temperatures ranged from very good to poor. Except for the very high gas temperature conditions (above $1667^{\circ}$ C ($3000^{\circ}$ F)) there did not seem to be a consistent trend in agreement (or disagreement) with gas temperature, gas pressure, or coolant temperature. In many instances, the agreement between the predicted and measured temperatures ranged from perfect to within $\pm 18^{\circ}$ C ($\pm 50^{\circ}$ F). Extreme disagreement, such as shown in figure 19 where the calculated temperature is about $267^{\circ}$ C ($480^{\circ}$ F) higher than the experimental values, is difficult to explain in view of the generally reasonable agreement for many other cases. One explanation may be the relatively small pressure differences that exist across the vane leading edge region (about 1.0 $N/cm^2$ (1.5 psi)) for the operating conditions of figure 19. Modest gas or coolant pressure fluctuations could materially affect the local coolant injection rates and consequently the surface temperature in the leading-edge region. Another factor contributing to the discrepancy might be radiant heat gain or loss.

Large errors in measured vane wall temperatures can lead to erroneous conclusions of blade and vane durability from the standpoint of oxidation, thermal fatigue, and stress rupture. For example, in figure 14 it can be seen that a difference of $111^{\circ}$ to $222^{\circ}$ C ($200^{\circ}$ to $400^{\circ}$ F) in the wall temperature of a Lamilloy vane made with Hastelloy-X material would have a significant effect on the coolant flow reduction expected for given operating times. Also for a material such as Hastelloy-X, a change of $55^{\circ}$ C ($100^{\circ}$ F) in its operating temperature can have a tenfold effect on its stress rupture life and significant effects on its yield strength (see ref. 6). Therefore, until improved experimental

techniques are obtained for defining the operating environment of blades and vanes, it will be difficult to accurately predict the life of the hardware. This is particularly true for operation at gas temperature levels above about 1371° C (2500° F), where radiation and gas luminosity can possibly affect vane and blade metal temperature measurements significantly.

Improvement in purely analytical approaches for predicting vane or blade airfoil temperatures is also required. Accurate definition of the airfoil operating environment is required (such as gas temperature distribution, static-pressure distribution, and velocity distribution). Better knowledge of the local blowing rates in porous materials in the presence of large static-pressure variations is required; better definition of coolant and gas-side heat-transfer coefficients is needed, and a better understanding of the boundary layer conditions around the airfoil is required.

It was not within the scope of the reference 3 investigation to make a thorough analysis of the experimental problems associated with accurately measuring gas temperatures and vane surface temperatures at elevated cascade gas temperature conditions. Likewise a thorough investigation of the problems associated with predicting surface temperatures of airfoils with a pseudo-transpiration-cooled material was not within the scope of the investigation. The results obtained do point out, however, that considerable improvement in experimental and analytical techniques is required.

## Thermal-Fatigue Tests

The thermal-fatigue tests consisted of a series of 3-minute cycles during which the gas temperature was maintained at a low level (616° C (1140° F)) for 90 seconds and at a high level (1538° C (2800° F)) for 90 seconds with ramp rates of 1.8 seconds between the two gas temperature levels. Figure 21 shows the typical time-temperature response during a single cycle that was obtained for the gas temperature, for the cooling air inlet temperature, and at a thermocouple on vane 3 located near the leading edge at a span distance 1.55 centimeters (0.61 in.) below midspan.

The cyclic tests were continued without interruption for 110 cycles, after which the cascade was shut down for a routine inspection of the vanes. Inspection revealed that all three test vanes had developed fatigue cracks. The exact number of cycles at which these failures occurred is unknown.

Figures 22 to 24 show the condition of vanes 2 to 4, respectively, after 110 cycles. It can be seen that vane 2 (fig. 22) exhibited the greatest fatigue damage, with a spanwise crack evident in the outer half of the vane leading edge (fig. 22(b)); numerous chordwise cracks emanating from the spanwise crack can also be observed. The chordwise cracks

in vane 3 (fig. 23) and vane 4 (fig. 24) were smaller but in the same general spanwise region.

The chordwise temperature distribution for the 3/4-span position of vane 3, where the peak metal temperatures and maximum chordwise temperature differences occurred, is shown in figure 25. These results were obtained by crossplotting the results from infrared photographs taken through the sight ports. The solid-line portion of each curve was faired through data points obtained from the infrared photographs. The dashed portions of the curves indicate the estimated temperature for regions of the vane for which experimental infrared photographic data were not available. These temperature results for the 3/4-span position are typical for all the test vanes.

Post-test thermal, structural, and metallurgical evaluations of the thermal-fatigue tests were made in an attempt to define the failure mechanism. These evaluations are discussed in the following sections.

Thermal analysis. - Thermal fatigue is strongly a function of variations in chordwise surface temperature distribution; therefore, the transient surface temperature response to a typical gas temperature cycle was predicted. This thermal prediction, as well as other studies of the failure mechanism, was made for vane 2, with particular emphasis on the structural behavior of the badly damaged 3/4-span position. The details of the transient vane metal temperature calculation procedure are given in reference 4.

The variation in gas temperature and coolant temperature during a typical cycle were based on experimentally measured values. The vane surface temperature distribution shown in figure 25 was assumed to be the initial temperature condition at the high gas temperature part of the cycle. The surface temperature distribution at the low gas temperature portion of the cycle was assumed to be uniform at a temperature of $344^{\circ}$ C ($710^{\circ}$ F). This assumption appeared to be reasonable based on available thermocouple readings; no infrared pictures could be taken at these low temperatures because the radiant energy levels were too low.

The predicted transient temperature response characteristics of vane 2 at the 3/4-span section are shown in figures 26 and 27 after a rapid decrease and increase in gas temperature, respectively. The results clearly indicate that the leading-edge response rates are significantly greater than those of the midchord region. This behavior reflects the relatively large leading-edge heat-transfer coefficients and is also indicative of the greater thermal inertia of the thicker walls in the midchord region. During the rapid gas temperature decrease (fig. 26), the leading-edge-to-midchord temperature difference goes from a large positive number (at 0 sec) to a negative number in 1 second. The maximum negative leading-edge-to-midchord temperature difference is reached in 2.2 seconds. During a rapid gas temperature increase (fig. 27), the leading-edge metal temperature increases more rapidly than for the other regions around the airfoil. These reversals of the temperature difference pattern between the leading edge and midchord

region of the vanes cause the thermal strains at the leading edge to cycle between large compressive and tensile values.

The results shown in figure 27 indicate that the predicted steady-state temperature distribution (solid curve for elapsed time of 30 sec) closely approximates the measured distribution (dashed curve). The small differences between the two curves reflect the error introduced by neglecting radial conduction effects in the calculation method.

The thermal gradients through the vane wall (from the gas-side surface to the coolant-side surface) also induce thermal strains which should be included in a structural analysis. These thermal gradients were estimated by the method discussed in reference 4 and taken into account in the structural analysis.

Structural analysis. - In order to thoroughly investigate the thermal cycling effect on airfoil life, a detailed structural analysis was made. The vane airfoil cross section was divided into 416 finite elements. Using the procedure discussed in reference 4, the total strain of each element at each loading condition was determined. The element which must withstand the greatest change in total strain during each cycle will be the one to fail. As the airfoil temperatures are cycled, the total strain ranges quickly stabilize to a fixed value for each cycle. For this investigation it was found that an element near the leading-edge stagnation point on the gas-side laminate had the greatest total strain excursion during a cycle.

The strain range at this leading-edge element was used to predict the number of thermal cycles to failure. The life was calculated by using the Method of Universal Slopes (ref. 12) and accounted for loading rate, stress concentration, and surface finish effects. The life was determined by using material properties for the two metal temperatures corresponding to the extremes of the strain range. In compression, the greatest strain occurred at a metal temperature of about $816^{\circ}$ C ($1500^{\circ}$ F); in tension, the corresponding temperature level was about $427^{\circ}$ C ($800^{\circ}$ F). The predicted cyclic life (time to initiation of a chordwise crack) of the leading-edge critical element was between 142 to 260 cycles.

A finite element analysis of this vane also indicated that the chordwise strains were only about 25 percent of the spanwise strains. Consequently, spanwise cracks were either secondary fatigue failures or resulted from other damage to the material, such as flaws introduced during fabrication.

Metallurgical evaluation. - After termination of the cyclic fatigue test, the three test vanes were removed from the cascade so that the type and mode of failure could be determined visually. The airfoils were sectioned in the relevant failure areas and the failure patterns were photographically recorded.

The following are the main points of the metallographic examination of the test vanes made in reference 4:

(1) Each of the failure surfaces examined revealed progressive fatigue failure.

(2) Plastic deformation (which probably occurred during the cold forming of the vane airfoil) was the primary cause of the spanwise crack failure along the leading edge of vane 2.

(3) The chordwise cracks in all three test vanes were partially transgranular and partially intergranular, indicative of thermal fatigue.

(4) No indications of delamination (bond failure) of the bonded sheets were evident.

Permeability results. - The permeability of the test vanes was measured before cycling and after 110 thermal cycles. Local permeabilities and overall flow through the vanes were evaluated. The local permeability data did not show any systematic changes in the airfoil flow - pressure drop characteristics after 110 thermal cycles. Where changes in local flow rate occurred, they were within the normal data scatter range for the test procedure used.

The overall vane airflow rates were obtained for a standard pressure drop of 6.89 $N/cm^2$ (10 psi) across the airfoil wall and an air temperature of $15^{\circ}$ C ($60^{\circ}$ F). A comparison of the overall flow rates before and after cycling are shown for the test vanes in the following table:

| Vane | Total vane flow rate | | | | Percent change |
|---|---|---|---|---|---|
| | Before cycling | | After cycling | | |
| | kg/sec | lb/sec | kg/sec | lb/sec | |
| 2 | 0.0296 | 0.0653 | 0.0363 | 0.0800 | 22 |
| 3 | .0309 | .0681 | .0250 | .0552 | -19 |
| 4 | .0341 | .0752 | .0325 | .0716 | -5 |

The large radial crack in the leading edge of vane 2 tends to explain the 22-percent flow increase. The flow decreases for vanes 3 and 4 may have resulted from oxidation or foreign matter collecting in the airfoil passages. The results are also somewhat in disagreement with the local permeability data; it should be noted, however, that the local permeability surveys covered considerably less than one-half of the airfoil surface area. The 5-percent decrease in flow for vane 4 is of the order of the measurement error.

It is believed that the relatively short overall operating time of vanes during the thermal cycling tests (about 5.5 hr) was too short to provide significant data relative to the effects of oxidation on the flow characteristics of Lamilloy under simulated engine operating conditions.

Suggested improvements. - The vanes investigated herein were designed for heat-transfer investigations in the static cascade. The internal stiffening sheets were dictated by cascade operational characteristics. Specifically, the vane wall reinforcement was designed to permit survival of the vane in the case of an emergency cascade

shutdown wherein the combustion gas pressure would decrease from its maximum value of about 96.5 $N/cm^2$ (140 psi) to 1 atmosphere, while the cooling air pressure (which was separately controlled) remained at a value of about 103.5 $N/cm^2$ (150 psi). This design condition is considerably more severe in terms of pressure differentials across the airfoil skin than would be encountered in an engine with the cooling air bled from the compressor.

This design requirement resulted in an airfoil wall that was unusually thick throughout the entire midchord region of the vane. A vane designed for engine application would be considerably thinner in the midchord region. A more nearly uniform wall thickness around the vane periphery would result in a more equitable distribution of wall stiffness. This would reduce the effects of side-wall load transfer to the thinner leading-edge region considerably. In addition, reduced overall wall thickness in the midchord regions would reduce the thermal inertia of the midchord walls. Consequently, the thermal "lag" of the vane side walls relative to the leading edge could be significantly reduced. The net effect would be to improve the thermal-fatigue life of the airfoil.

An improved fabrication technique such as a hot creep forming process would alleviate the deformation and cracking problems attributable to cold forming of the airfoils.

As a result of these and other investigations, improvements in the internal cooling characteristics of Lamilloy were evolved by the Detroit Diesel Allison Division of General Motors. Lamilloy vanes now utilize impingement cooling at the leading-edge region to reduce the chordwise surface temperature variation and, therefore, increase the thermal-fatigue life.

## GENERAL COMMENTS

The selection of a cooling configuration for a particular airfoil application involves a number of design tradeoffs. For example, material cost, oxidation characteristics, cooling air flow requirements, weight, strength, and life characteristics must all be considered in the selection of a cooling scheme.

Lamilloy has excellent oxidation characteristics and a fairly high value (0.6 to 0.7) for the cooling performance parameter $\varphi$. Also, a blade or vane fabricated from Lamilloy would be relatively light. Some disadvantages of Lamilloy include low strength relative to certain cast materials and possibly relatively high cost.

WPM vanes or blades possibly would be cheaper than Lamilloy, but they would require internal struts for support and metering of the airflow to the various sections of the airfoil. The struts result in heavier blades and rotor disks, and, therefore, a weight penalty on the engine. Also, the WPM exhibited a lower resistance to clogging due to internal flow passage oxidation than did Lamilloy, when both materials were made from

Hastelloy-X alloy. However, other oxidation resistant alloys have been developed that can be used in the fabrication of WPM (ref. 11) which virtually eliminate the oxidation clogging problem with WPM. These alloys are relatively weak and are more likely to require internal struts than Lamilloy blades or vanes made from less oxidation resistant, but stronger, sheet materials.

Casting is the most convenient and least expensive method for mass producing turbine vanes and blades. The cooling configurations that may be cast are limited to relatively simple configurations with lower cooling performance than porous configurations fabricated from wire-mesh or sheet-metal laminates. The cooling performance parameter $\varphi$ for a typical film-cooled cast blade is about 0.5. Casting materials are much stronger in stress rupture than sheet materials for the metal temperatures and centrifugal stress conditions typical of rotor blades in advanced airbreathing engines.

A brief analytical study was made at the Lewis Research Center in which sheet metal blades made from Udimet 700 (the strongest sheet material for rotor blades for which the authors could find material properties in the literature) were compared with a typical film-cooled blade cast from IN-100. Blade lives were calculated by using the stress relaxation program described in reference 13, which considers the effect of centrifugal and gas forces, thermal stresses, creep, and plastic flow. The results indicated that if both blades had a $\varphi$ of 0.5, the sheet-metal blade life would be about 10 percent of the cast blade life. The analysis also showed that if the sheet-metal blade had a $\varphi$ of about 0.77, the lives of the two blades would be about the same. Lamilloy vanes have demonstrated $\varphi$-values between 0.6 and 0.7. Therefore, further improvements will be required in the cooling performance or in sheet-metal technology to make Lamilloy blades competitive with cast rotor blades with simpler cooling configurations. Other tradeoffs, such as weight, turbine inlet temperature, and coolant flow rate can be made between sheet-metal and cast rotor blade construction, but it can be expected that most of these tradeoffs will be in favor of cast blades as long as the large strength advantage remains with cast materials and high blade strength and life is a major requirement. Lamilloy may have potential advantages over cast configurations for very high gas temperature levels where coolant requirements may become prohibitive for cooling methods other than transpiration (or pseudotranspiration) cooling. Lamilloy may also show an advantage over cast configurations in engine applications involving short engine life where strength is not a prime factor.

## SUMMARY OF RESULTS

An experimental investigation was made to obtain the fluid flow, oxidation, and strength characteristics of Lamilloy (a laminated porous sheet material) and a wire-wound type of porous material. Both materials were made from the same nickel-base

alloy, namely Hastelloy-X. A vane configuration made from Lamilloy was designed for investigation in a static cascade facility. The cooling performance of vanes made from Lamilloy was obtained in a five-vane static cascade facility that was operated at nominal gas temperatures that ranged from 1093° to 1649° C (2000° to 3000° F). A thermal-fatigue investigation was also made in the static cascade. Three test vanes were subjected to 3-minute thermal cycles wherein the gas temperature was rapidly increased and decreased from 617° C (1140° F) and 1537° C (2800° F), respectively. The principal results obtained were as follows:

1. The flow characteristics of Lamilloy were correlated by using Green's equation, which was developed for other porous materials (such as wireform and powdered sintered porous materials). Data taken over a range of pressure, temperature, and mass flows and for 15 different geometries were correlated.

2. Lamilloy that was exposed to an oxidizing-type atmosphere was significantly less sensitive to flow reductions than was the wire-wound porous material when both Lamilloy and the wire-wound porous material were made of Hastelloy-X and exposed to the same conditions.

3. The experimental cooling investigation of vanes made from Lamilloy in a static cascade indicated that the peak airfoil surface temperature consistently occurred at the leading-edge region. The midchord suction surface temperatures were generally 111° to 167 C° (200 to 300 F°) lower than the peak temperatures. The pressure surface temperatures were higher than the suction surface temperatures and generally showed a steady decrease in temperature with distance from the leading edge. The maximum vane surface temperature observed for any cascade operating condition was 882° C (1620° F). The value of the cooling performance parameter $\varphi$ of the Lamilloy vanes was approximately 0.6 to 0.7 over the range of test conditions investigated.

4. Comparison of predicted airfoil metal temperatures with those measured experimentally ranged from good to poor. The general trends of the metal temperature distributions were predicted fairly well in some cases. The greatest disagreement between measured and predicted temperatures occurred at the high temperature levels; the predicted temperatures were as much as 267° C (480° F) higher than the measured values at the leading edge.

5. The three vanes subjected to rapid thermal transients were found to be cracked in the airfoil leading-edge region when first inspected after 110 cycles. The exact time when these cracks occurred is unknown. Chordwise cracks found in all three test vanes were caused by thermal fatigue as a result of large chordwise temperature gradients in the vane airfoils. A large spanwise crack observed in one vane was believed to have been caused primarily by the cold forming process used in the fabrication of the airfoils.

6. A thermal-fatigue analysis, which was applied to the vanes for the operating conditions of the cascade, predicted failure of the vanes between 142 and 260 cycles.

Lewis Research Center,
National Aeronautics and Space Administration,
Cleveland, Ohio, November 2, 1971,
764-74.

# APPENDIX - SYMBOLS

$C_f$ flow resistance factor (eq. (4))

$D_h$ hydraulic diameter at minimum construction

G mass flow rate of coolant through vane wall (or specimen) per unit area

$G_{10}$ standard flow rate calculated from eq. (1) for $P_1 = 17.0$ N/cm$^2$ (24.7 psia), $P_2 = 10.1$ N/cm$^2$ (14.7 psia), and $T = 24^\circ$ C ($75^\circ$ F)

g gravitational constant

HS spacing between holes in square array

$K'/\tau$ permeability, $2RT\mu G_{10}/(P_1^2 - P_2^2)$, where $P_1 = 17.0$ N/cm$^2$ (24.7 psia), $P_2 = 10.1$ N/cm$^2$ (14.7 psia), and $T = 24^\circ$ C ($75^\circ$ F)

$P_1$ internal static pressure

$P_2$ external static pressure

R universal gas constant

Re Reynolds number in flow specimen or blade wall (eq. (4))

T temperature of air

$T_c$ cooling air inlet temperature

$T_g$ effective gas temperature

$T_T$ free-stream total temperature

$T_w$ surface metal temperature

t time

$W_c$ coolant mass flow rate

$W_g$ combustion gas mass flow rate

$\alpha$ porous wall viscous resistance coefficient

$\beta$ porous wall inertial resistance coefficient

$\delta$ ratio of combustion gas total pressure to NASA standard sea-level pressure

$\varphi$ $(T_T - T_w)/(T_T - T_c)$

$\theta$ ratio of combustion gas total temperature to NASA standard sea-level temperature

$\mu$ cooling air viscosity

$\tau$ thickness of vane wall

# REFERENCES


1. Helms, H. E.; and Emmerson, C. W.: Analysis and Testing of Air-Cooled Turbine Rotor and Stator Blades. Paper 65-WA/GTP-10, ASME, Nov. 1965.

2. Anderson, R. D.; and Nealy, D. A.: Evaluation of Laminated Porous Material for High-Temperature Air-Cooled Turbine Blades. Rep. EDR-4968, Allison Division, General Motors (NASA CR-72281), Jan. 16, 1967.

3. Nealy, D. A.; Anderson, R. D.; and Hufford, A. A.: Design and Experimental Evaluation of a Turbine Vane Fabricated from Laminated Porous Material. Rep. EDR-6296, Allison Division, General Motors (NASA CR-72649), July 31, 1969.

4. Nealy, D. A.; Anderson, R. D.; and Hufford, A. A.: Experimental Evaluation of Low Cycle Thermal Fatigue in a Turbine Vane Fabricated from Laminated Porous Material. Rep. EDR-7034, Allison Division, General Motors (NASA CR-72954), Mar. 15, 1971.

5. Wheeler, H. L., Jr.: Transpiration Cooling in High Temperature Gas Turbine. Bendix Filter Div., Bendix Corp., Mar. 1964.

6. Anon.: High Temperature, High Strength, Nickel Base Alloys. International Nickel Co., 1964.

7. Whitney, Warren J.; Szanca, Edward M.; Moffitt, Thomas P.; and Monroe, Daniel E.: Cold-Air Investigation of a Turbine for High-Temperature-Engine Application. NASA TN D-3751, 1967.

8. Goodbar, W. L.: An Improved Method for Measuring Turbine Vane Temperature in Hot Cascade Rigs. Paper 66-642, AIAA, June 1966.

9. Green, Leon, Jr.; Duwez, Pol: Fluid Flow Through Porous Metals. J. Appl. Mech., vol. 18, no. 1, Mar. 1951, pp. 39-45.

10. Kaufman, Albert; and Richards, Hadley T.: Investigation of Flow Characteristics of Some Wire-Form and Laminate-Form Materials. NASA TM X-2111, 1970.

11. Esgar, Jack B.; Colladay, Raymond S.; and Kaufman, Albert: An Analysis of the Capabilities and Limitations of Turbine Air Cooling Methods. NASA TN D-5992, 1970.

12. Manson, S. S.: Fatigue: A Complex Subject - Some Simple Approximations. Experimental Mech., vol. 5, no. 7, July 1965, pp. 193-226.

13. Kaufman, Albert: Steady-State Stress Relaxation Analysis of Turbine Blade Cooling Designs. NASA TN D-5282, 1969.

TABLE I. - GEOMETRY STUDY MATERIAL DEFINITION

| Configuration | Laminate | Laminate thickness | | Grid array | Grid depth | | Hole diameter | | Hole spacing | | Overall thickness | | Grid spacing | | Land diameter | |
|---|---|---|---|---|---|---|---|---|---|---|---|---|---|---|---|---|
| | | cm | in. | | cm | in. | cm | in. | cm | in. | cm | in. | cm | in. | cm | in. |
| 1 | 1 | 0.0206 | 0.0081 | Standard | 0.0097 | 0.0038 | 0.038 | 0.015 | 0.244 | 0.096 | 0.0622 | 0.0245 | 0.061 | 0.024 | 0.061 | 0.024 |
| | 2 | .0203 | .0080 | Standard | .0097 | .0038 | .038 | .015 | .244 | 096 | | | | | | |
| | 3 | .0203 | .0080 | | | | .041 | .016 | .244 | .096 | | | | | | |
| 2 | 1 | 0.0203 | 0.0080 | Standard | 0.0091 | 0.0036 | 0.048 | 0.019 | 0.244 | 0.096 | 0.0622 | 0.0245 | 0.061 | 0.024 | 0.056 | 0.022 |
| | 2 | .0203 | .0080 | Standard | .0091 | .0036 | .046 | .018 | .244 | .096 | | | | | | |
| | 3 | .0203 | .0080 | | | | .043 | .017 | .244 | .096 | | | | | | |
| 3 | 1 | 0.0203 | 0.0080 | Standard | 0.0102 | 0.0040 | 0.058 | 0.023 | 0.244 | 0.096 | 0.0622 | 0.0245 | 0.061 | 0.024 | 0.064 | 0.025 |
| | 2 | .0203 | .0080 | Standard | .0102 | .0040 | .058 | .023 | .244 | .096 | | | | | | |
| | 3 | .0203 | .0080 | | | | .064 | .025 | .244 | .096 | | | | | | |
| 4 | 1 | 0.0203 | 0.0080 | Standard | 0.0102 | 0.0040 | 0.046 | 0.018 | 0.122 | 0.048 | 0.0627 | 0.0247 | 0.061 | 0.024 | 0.043 | 0.017 |
| | 2 | .0203 | .0080 | Standard | .0102 | .0040 | .043 | .017 | .122 | .048 | | | | | | |
| | 3 | .0203 | .0080 | | | | .041 | .016 | .122 | .048 | | | | | | |
| 5 | 1 | 0.0203 | 0.0080 | Standard | 0.0102 | 0.0040 | 0.048 | 0.019 | 0.366 | 0.144 | 0.0622 | 0.0245 | 0.061 | 0.024 | 0.056 | 0.022 |
| | 2 | .0203 | .0080 | Standard | .0099 | .0039 | .046 | .018 | .366 | .144 | | | | | | |
| | 3 | .0203 | .0080 | | | | .046 | .018 | .366 | .144 | | | | | | |
| 6 | 1 | 0.0102 | 0.0040 | Standard | 0.0053 | 0.0021 | 0.038 | 0.015 | 0.244 | 0.096 | 0.0330 | 0.0130 | 0.061 | 0.024 | 0.064 | 0.025 |
| | 2 | .0102 | .0040 | Standard | .0056 | .0022 | .041 | .016 | .244 | .096 | | | | | | |
| | 3 | .0102 | .0040 | | | | .036 | .014 | .244 | .096 | | | | | | |
| 7 | 1 | 0.0206 | 0.0081 | Standard | 0.0051 | 0.0020 | 0.046 | 0.018 | 0.244 | 0.096 | 0.0622 | 0.0245 | 0.061 | 0.024 | 0.056 | 0.022 |
| | 2 | .0208 | .0082 | Standard | .0051 | .0020 | .046 | .018 | .244 | .096 | | | | | | |
| | 3 | .0208 | .0082 | | | | .046 | .018 | .244 | .096 | | | | | | |
| 8 | 1 | 0.0323 | 0.0127 | Standard | 0.0117 | 0.0046 | 0.053 | 0.021 | 0.244 | 0.096 | 0.0940 | 0.0370 | 0.061 | 0.024 | 0.053 | 0.021 |
| | 2 | .0323 | .0127 | Standard | .0117 | .0046 | .053 | .021 | .244 | .096 | | | | | | |
| | 3 | .0315 | .0124 | | | | .046 | .018 | .244 | .096 | | | | | | |
| 9 | 1 | 0.0203 | 0.0080 | Standard | 0.0102 | 0.0040 | 0.048 | 0.019 | 0.244 | 0.096 | 0.1029 | 0.0405 | 0.061 | 0.024 | 0.051 | 0.020 |
| | 2 | .0201 | .0079 | Standard | .0102 | .0040 | .048 | .019 | .244 | .096 | | | | | | |
| | 3 | .0203 | .0080 | Standard | .0102 | .0040 | .048 | .019 | .244 | .096 | | | | | | |
| | 4 | .0203 | .0080 | Standard | .0099 | .0039 | .046 | .018 | .244 | .096 | | | | | | |
| | 5 | .0203 | .0080 | | | | .046 | .018 | .244 | .096 | | | | | | |
| 10 | 1 | 0.0208 | 0.0082 | Modified standard | 0.0094 | 0.0037 | 0.038 | 0.015 | 0.244 | 0.096 | 0.0622 | 0.0245 | 0.041 | 0.016 | 0.041 | 0.015 |
| | 2 | .0206 | .0081 | Modified standard | .0091 | .0036 | .038 | .015 | .244 | .096 | | | | | | |
| | 3 | .0208 | .0082 | | | | .041 | .016 | .244 | .096 | | | | | | |
| 11 | 1 | 0.0208 | 0.0082 | Connected | 0.0102 | 0.0040 | 0.036 | 0.014 | 0.244 | 0.096 | 0.0622 | 0.0245 | 0.041 | 0.016 | 0.036 | 0.014 |
| | 2 | .0206 | .0081 | Connected | .0102 | .0040 | .036 | .014 | .244 | .096 | | | | | | |
| | 3 | .0208 | .0082 | | | | .038 | .015 | .244 | .096 | | | | | | |
| 12 | 1 | 0.0203 | 0.0080 | Standard | 0.0076 | 0.0030 | 0.046 | 0.018 | 0.244 | 0.096 | 0.0622 | 0.0245 | 0.061 | 0.024 | 0.058 | 0.023 |
| | 2 | .0201 | .0079 | Standard | .0076 | .0030 | .046 | .018 | .244 | .096 | | | | | | |
| | 3 | .0206 | .0081 | | | | .046 | .018 | .244 | .096 | | | | | | |
| 13 | 1 | 0.0206 | 0.0081 | Standard | 0.00241 | 0.00095 | 0.043 | 0.017 | 0.244 | 0.096 | 0.0622 | 0.0245 | 0.061 | 0.024 | 0.066 | 0.026 |
| | 2 | .0206 | .0081 | Standard | .00241 | .00095 | .046 | .018 | .244 | .096 | | | | | | |
| | 3 | .0203 | .0080 | | | | .046 | .018 | .244 | .096 | | | | | | |
| 14 | 1 | 0.0201 | 0.0079 | Standard | 0.0051 | 0.0020 | 0.038 | 0.015 | 0.366 | 0.144 | 0.0610 | 0.0240 | 0.061 | 0.024 | 0.061 | 0.024 |
| | 2 | .0201 | .0079 | Standard | .0048 | .0019 | .038 | .015 | .366 | .144 | | | | | | |
| | 3 | .0206 | .0081 | | | | .038 | .015 | .366 | .144 | | | | | | |
| 15 | 1 | 0.0203 | 0.0080 | Standard | 0.0051 | 0.0020 | 0.043 | 0.017 | 0.122 | 0.048 | 0.0622 | 0.0245 | 0.061 | 0.024 | 0.056 | 0.022 |
| | 2 | .0206 | .0081 | Standard | .0051 | .0020 | .043 | .017 | .122 | .048 | | | | | | |
| | 3 | .0203 | .0080 | | | | .043 | .017 | .122 | .048 | | | | | | |

TABLE II. - NOMINAL CASCADE TEST CONDITIONS FOR COOLING PERFORMANCE INVESTIGATION

| Average total inlet gas temperature | | Average total inlet gas pressure | | Cooling air temperature | |
|---|---|---|---|---|---|
| $^{o}C$ | $^{o}F$ | $N/cm^2$ | psia | $^{o}C$ | $^{o}F$ |
| 1093 | 2000 | 78.6 | 114 | 316 | 600 |
| 1232 | 2250 | ↓ | ↓ | ↓ | ↓ |
| 1371 | 2500 | | | | |
| 1510 | 2750 | | | | |
| 1649 | 3000 | | | | |
| 1093 | 2000 | | | 454 | 850 |
| 1232 | 2250 | | | ↓ | ↓ |
| 1371 | 2500 | | | | |
| 1510 | 2750 | ↓ | ↓ | | |
| 1371 | 2500 | 96.6 | 140 | 316 | 600 |

TABLE III. - PERMEABILITY DATA FOR LAMILLOY GEOMETRY INVESTIGATION

| Configuration | Viscous resistance coefficient | | Inertial resistance coefficient | | Permeability-coefficient-to-thickness ratio | |
|---|---|---|---|---|---|---|
| | $cm^{-2}$ | $in.^{-2}$ | $cm^{-1}$ | $in.^{-1}$ | m | ft |
| 1 | $5.42\times10^{7}$ | $34.99\times10^{7}$ | $3.45\times10^{5}$ | $8.77\times10^{5}$ | $3.545\times10^{-10}$ | $11.63\times10^{-10}$ |
| 2 | 4.86 | 31.38 | 2.22 | 5.63 | 4.389 | 14.40 |
| 3 | .927 | 5.98 | 2.85 | 7.24 | 4.106 | 13.47 |
| 4 | .047 | .30 | .087 | .22 | 23.48 | 77.02 |
| 5 | .39 | 67.06 | 11.49 | 29.19 | 1.94 | 6.35 |
| 6 | 33.35 | 215.14 | 16.20 | 41.16 | 2.10 | 6.88 |
| 7 | 24.86 | 160.41 | 9.07 | 23.04 | 1.95 | 6.39 |
| 8 | .246 | 1.59 | .756 | 1.92 | 6.511 | 21.36 |
| 9 | 4.39 | 28.32 | 1.40 | 3.55 | 4.161 | 13.65 |
| 10 | 5.00 | 32.23 | 3.85 | 9.79 | 3.380 | 11.09 |
| 11 | 4.75 | 30.62 | 4.58 | 11.64 | 3.124 | 10.25 |
| 12 | 4.40 | 28.39 | 3.64 | 9.25 | 3.496 | 11.47 |
| 13 | 303.92 | 1960.80 | 93.15 | 236.59 | .381 | 1.25 |
| 14 | 127.50 | 822.57 | 123.03 | 312.19 | .500 | 1.64 |
| 15 | 2.01 | 12.97 | .567 | 1.44 | 8.793 | 28.85 |

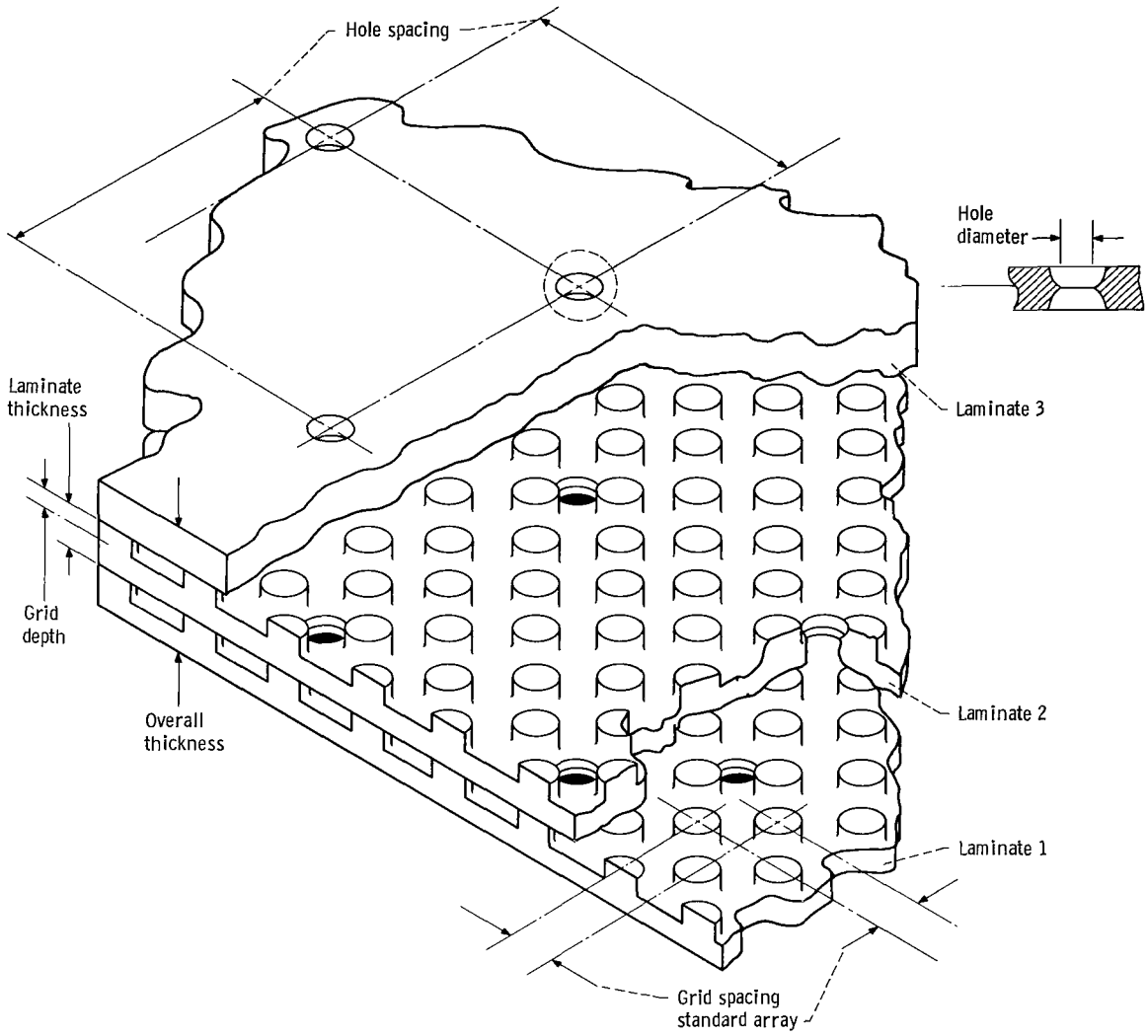


(a) Circular pedestal grid array.

Figure 1. - Schematic diagram of typical Lamilloy porous material.

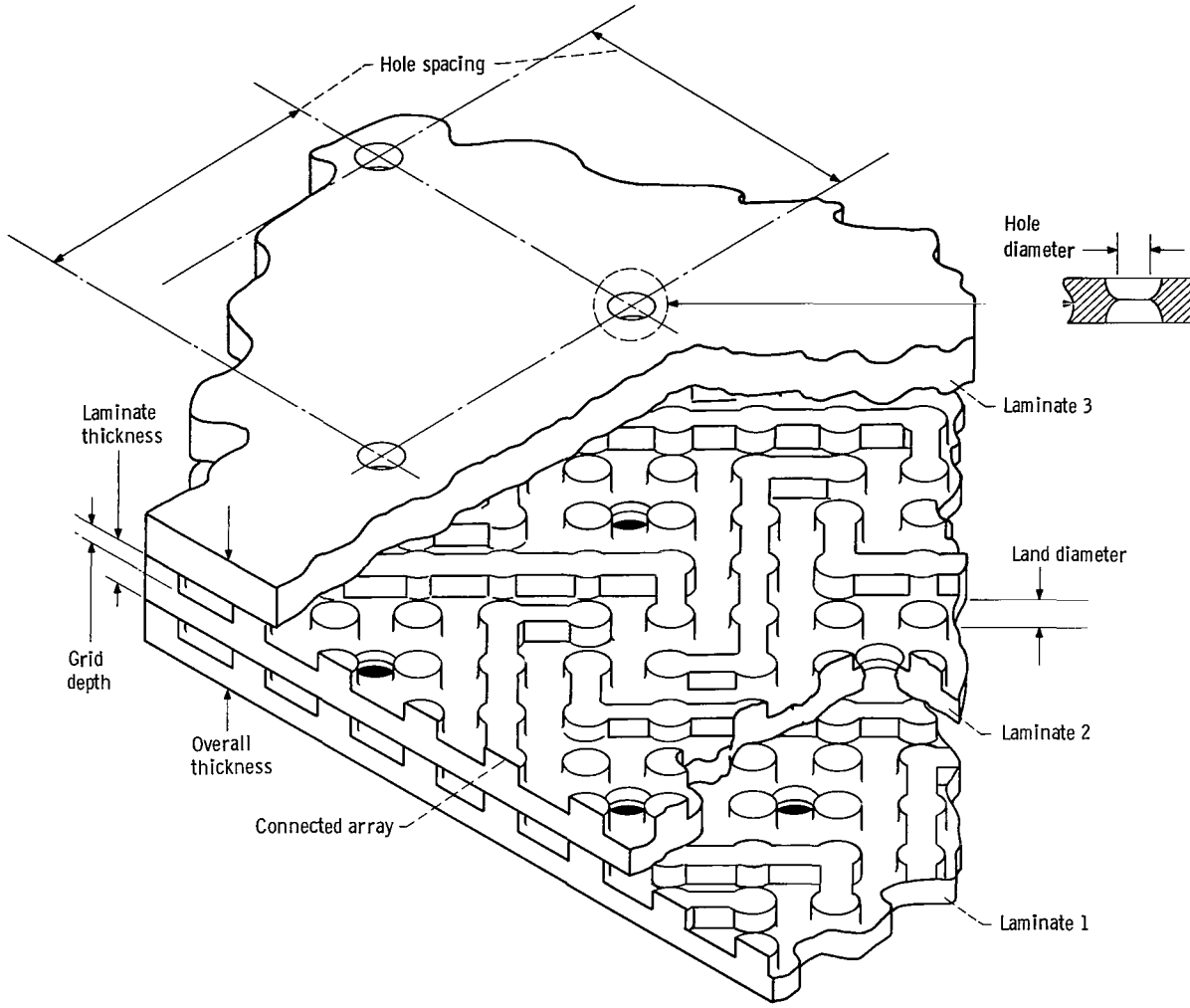


(b) Connected grid array.

Figure 1. - Concluded.

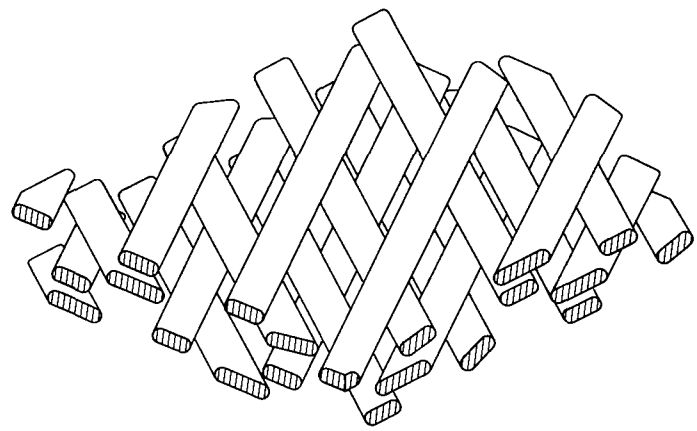

Figure 2. - Schematic of typical wire-wound porous material configuration.

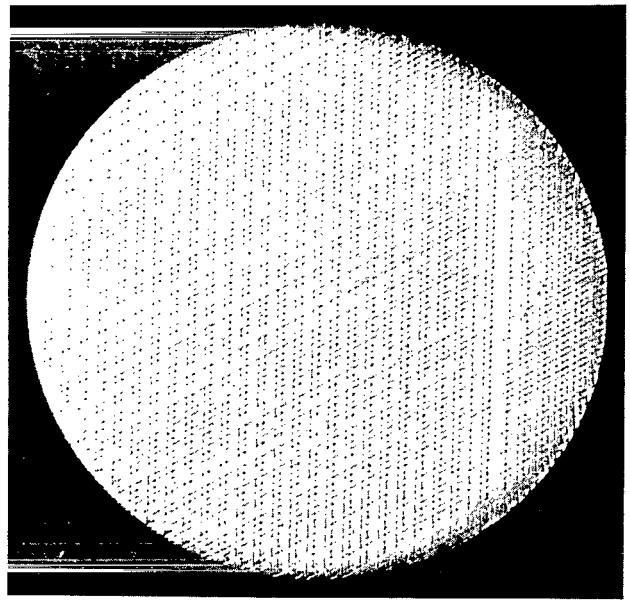

(a) Wire-wound porous material.

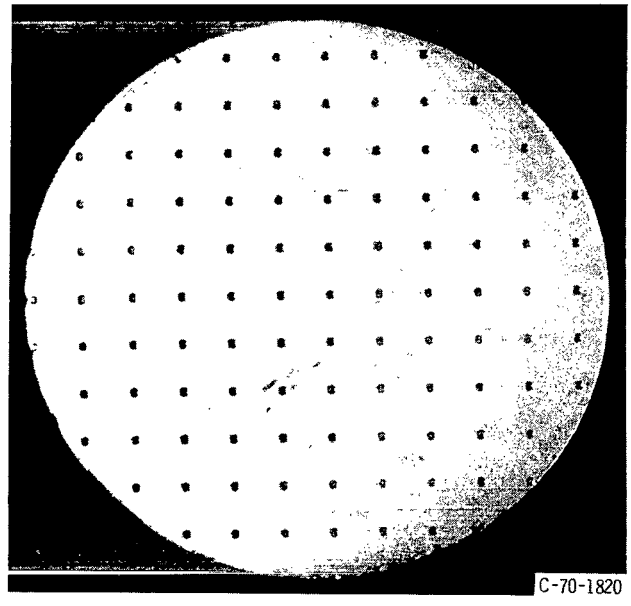


(b) Lamilloy material.

Figure 3. - Disk-type flow specimens.

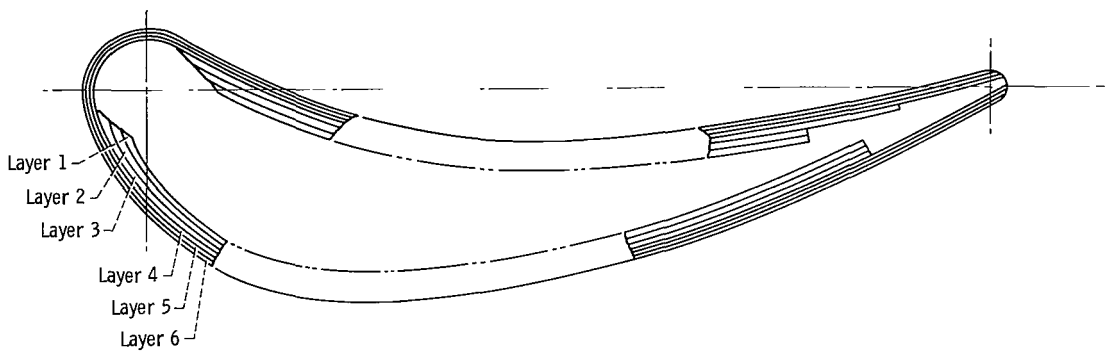


(a) Cross section of formed vane. Layers 1, 2, and 3 were added for stiffening; layers 4, 5, and 6 form the heat-transfer portion of the wall.

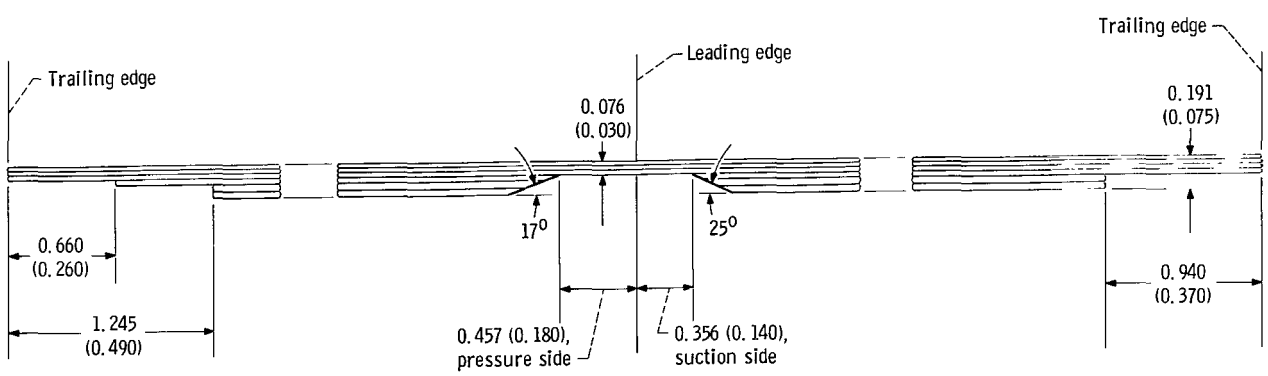


(b) Cross section of Lamilloy material before forming. Dimensions are in centimeter (in.).

Figure 4. - Cross section of Lamilloy porous material vane.

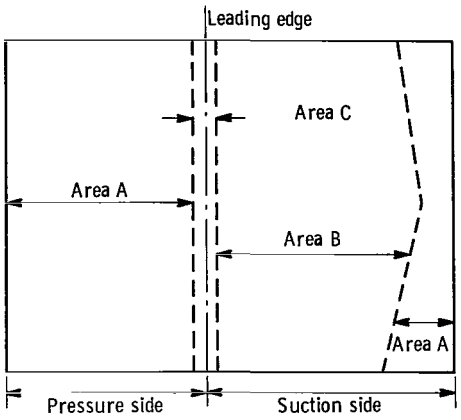


| Area | Viscous resistance coefficient, $\alpha$ | | Inertial resistance coefficient, $\beta$ | | Flow rate parameter range, $G_c/\mu_c$ | |
|---|---|---|---|---|---|---|
| | $cm^{-2}$ | $in.^{-2}$ | $cm^{-1}$ | $in.^{-1}$ | $cm^{-1}$ | $in.^{-1}$ |
| A | $1.35 \times 10^9$ | $0.21 \times 10^9$ | $27.4 \times 10^5$ | $10.8 \times 10^5$ | 3771 to 11 375 | 1485 to 4620 |
| B | 3.87 | .60 | 18.39 | 7.24 | 6172 to 16 154 | 2430 to 6360 |
| C | 1.94 | .30 | 2.21 | .87 | 9525 to 17 780 | 3750 to 7000 |

Figure 5. - Developed view of airfoil sheet showing areas of constant permeability.

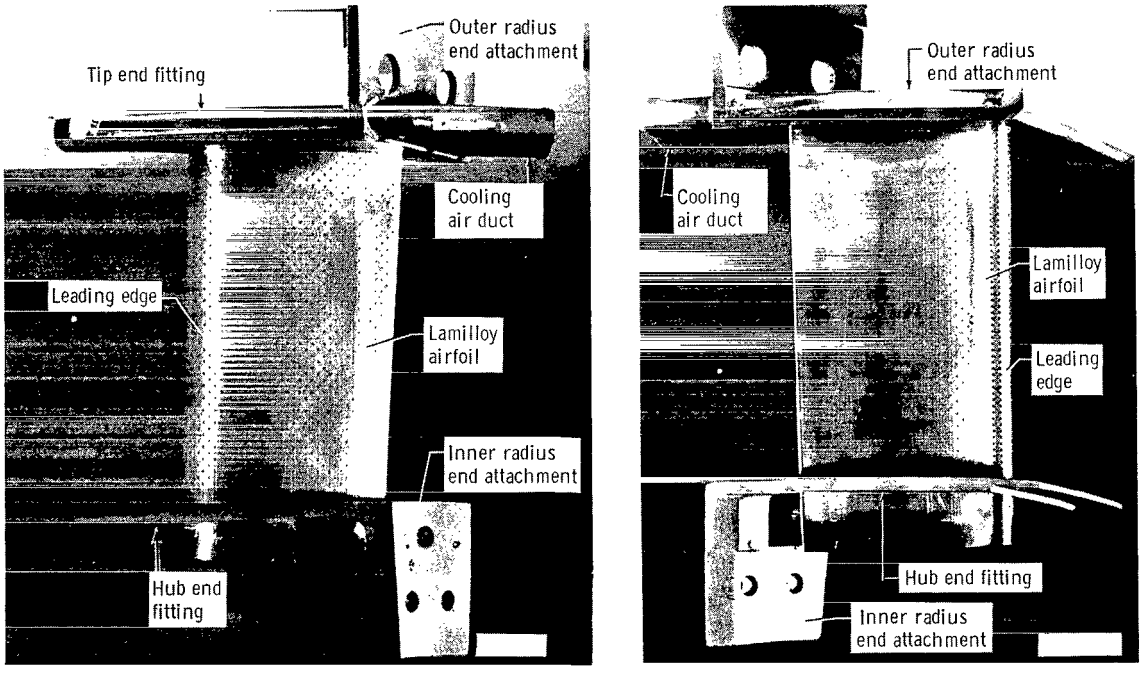


(a) Suction surface.

(b) Pressure surface.

Figure 6. - Lamilloy porous material vane.

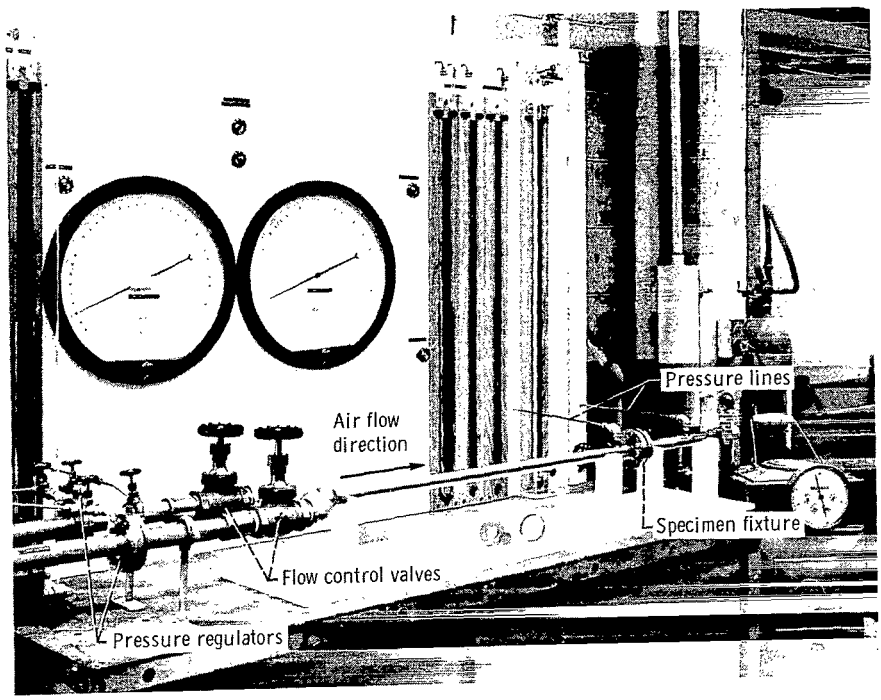


(a) Rig assembly.

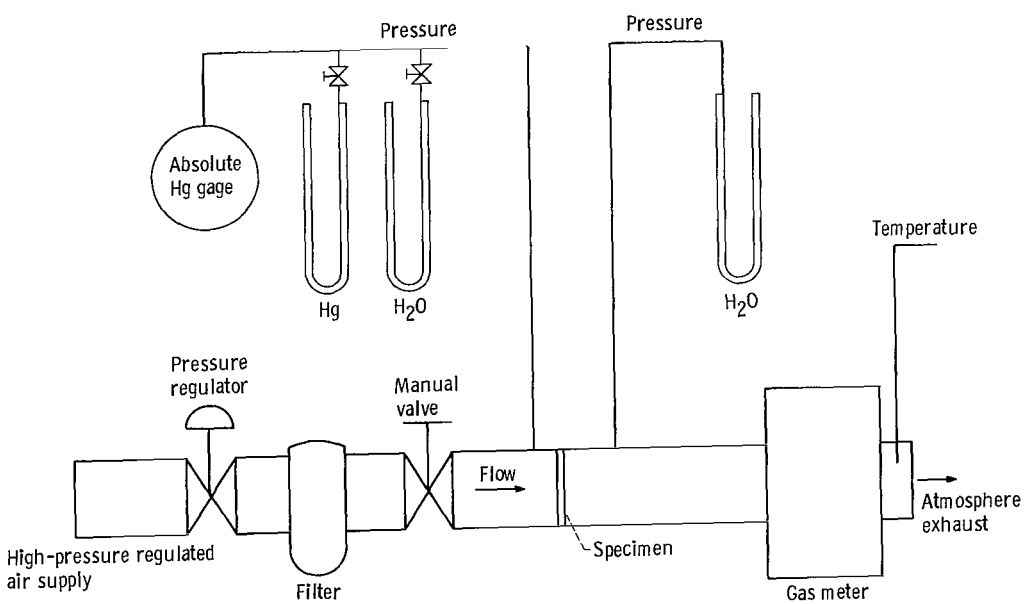


(b) Schematic of flow system.

Figure 7. - Ambient-temperature permeability test apparatus.

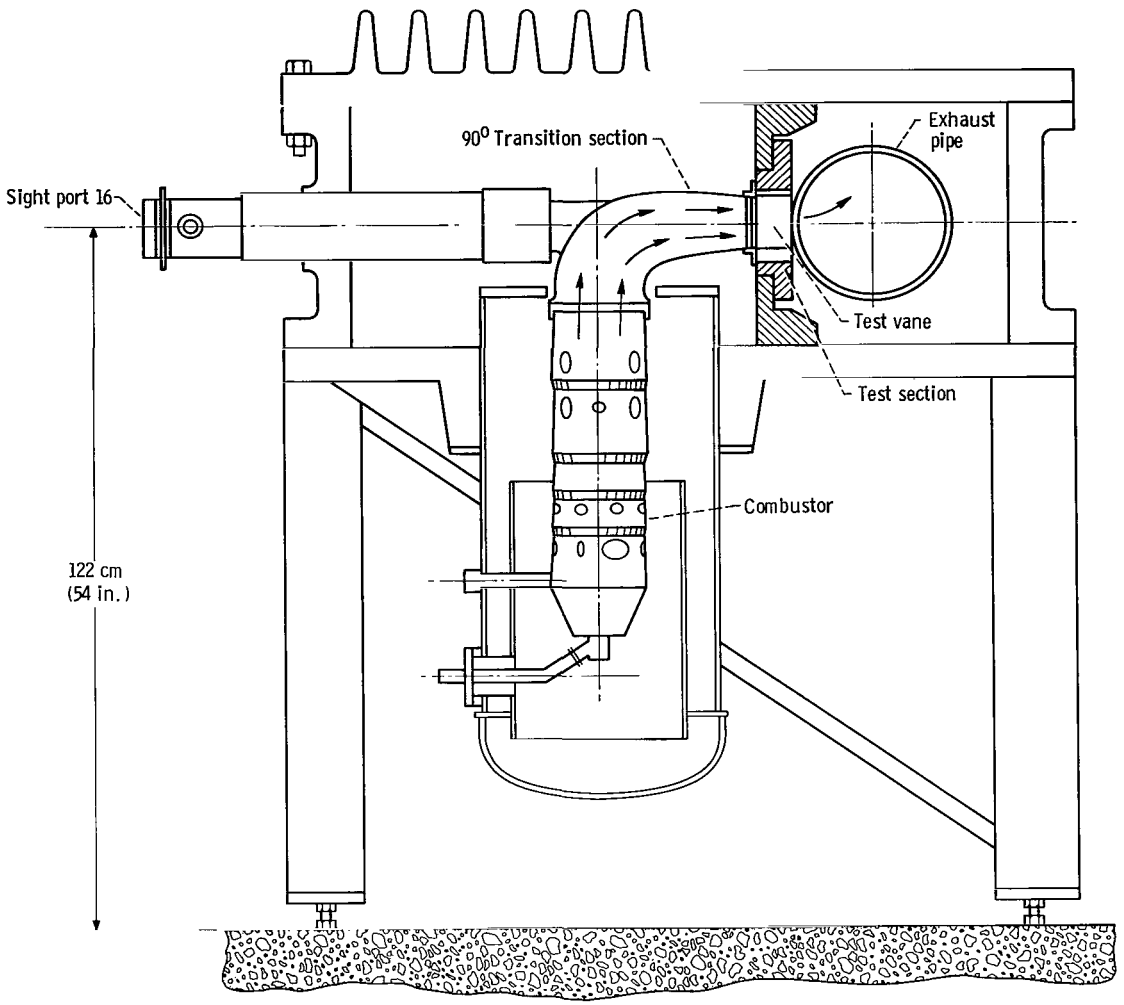


(a) Side view.

Figure 8. - Schematic of hot cascade test facility.

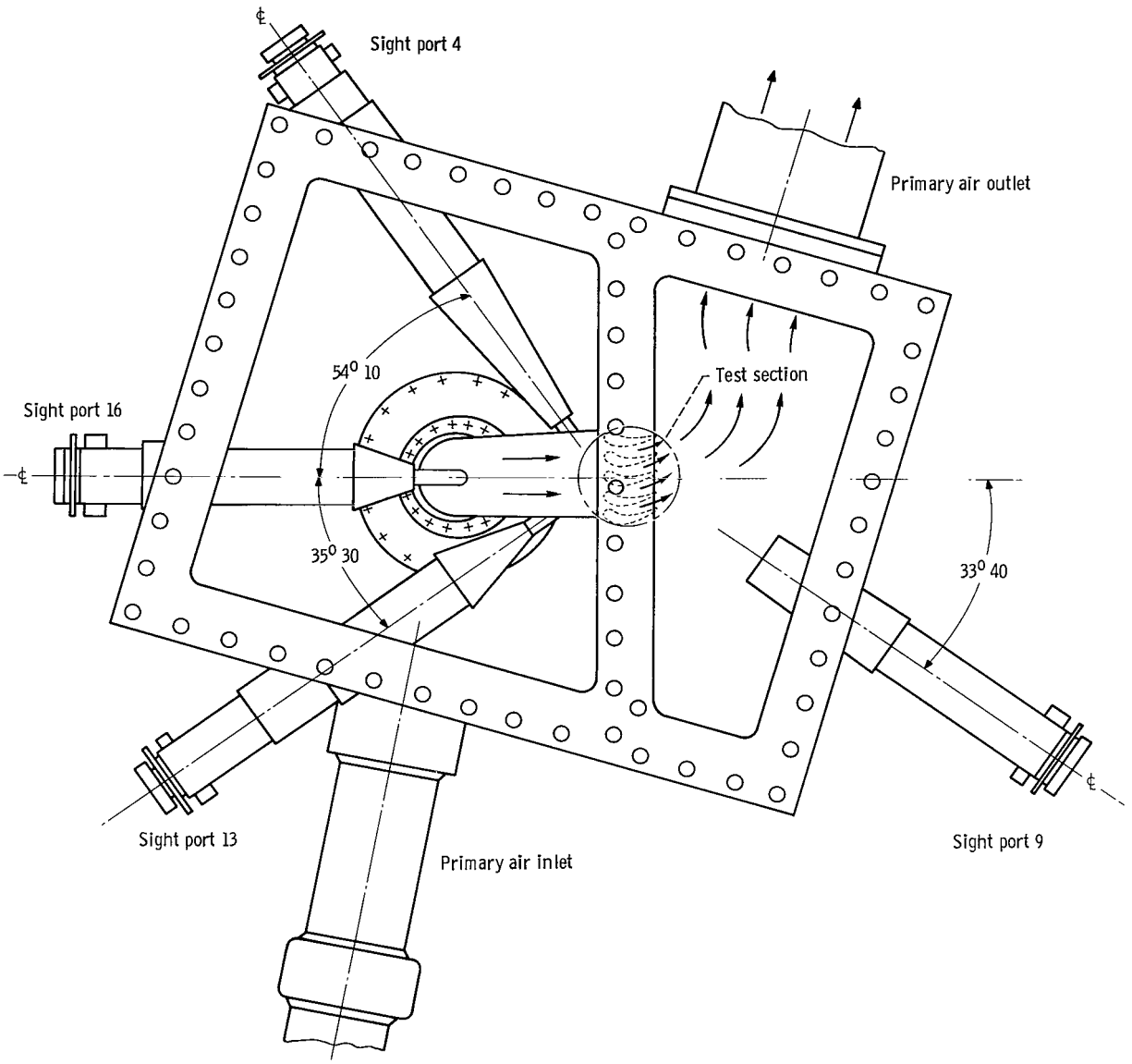


(b) Top view

Figure 8. - Concluded

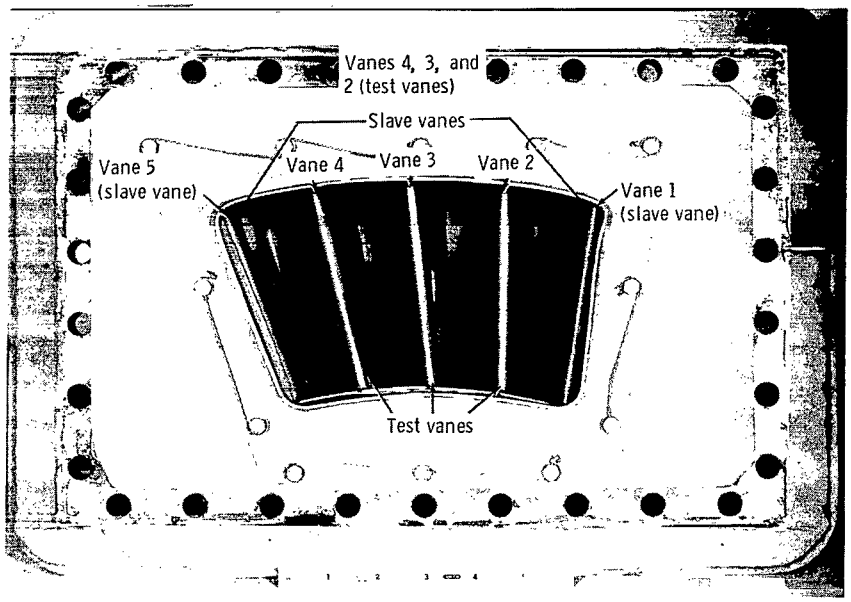


Figure 9. - Leading-edge view of vanes mounted in test fixture.

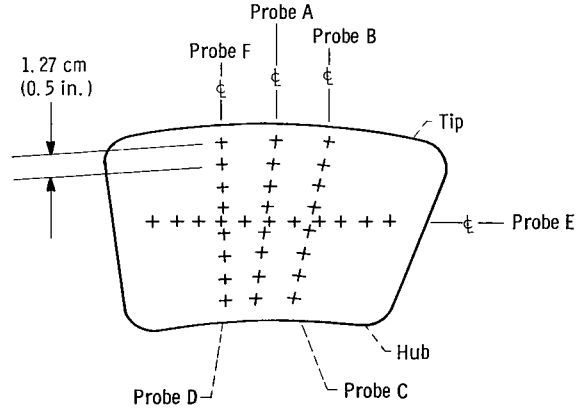


Figure 10. - Gas temperature thermocouple locations. Probes A, B, E, and F are traversing type; and probes C and D are fixed. Probes A, B, and F are 6.04 centimeters (2.38 in.) upstream of vane leading edge, while probes C, D, and E are 7.65 centimeters (3.01 in.) upstream.

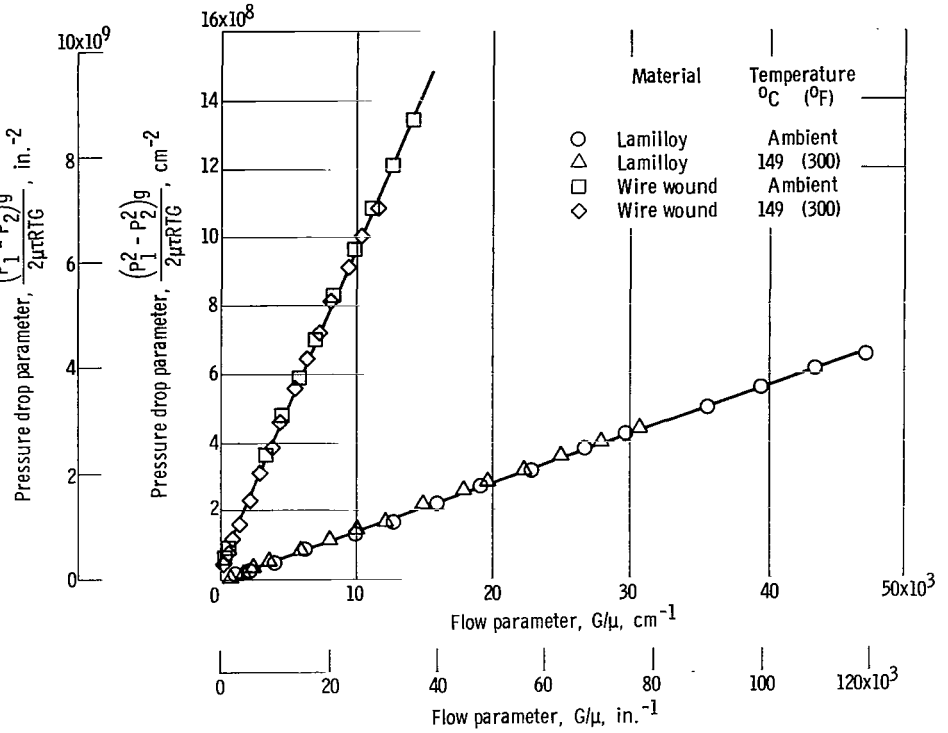


Figure 11. - Typical permeability data for a high-flow-level porous material.

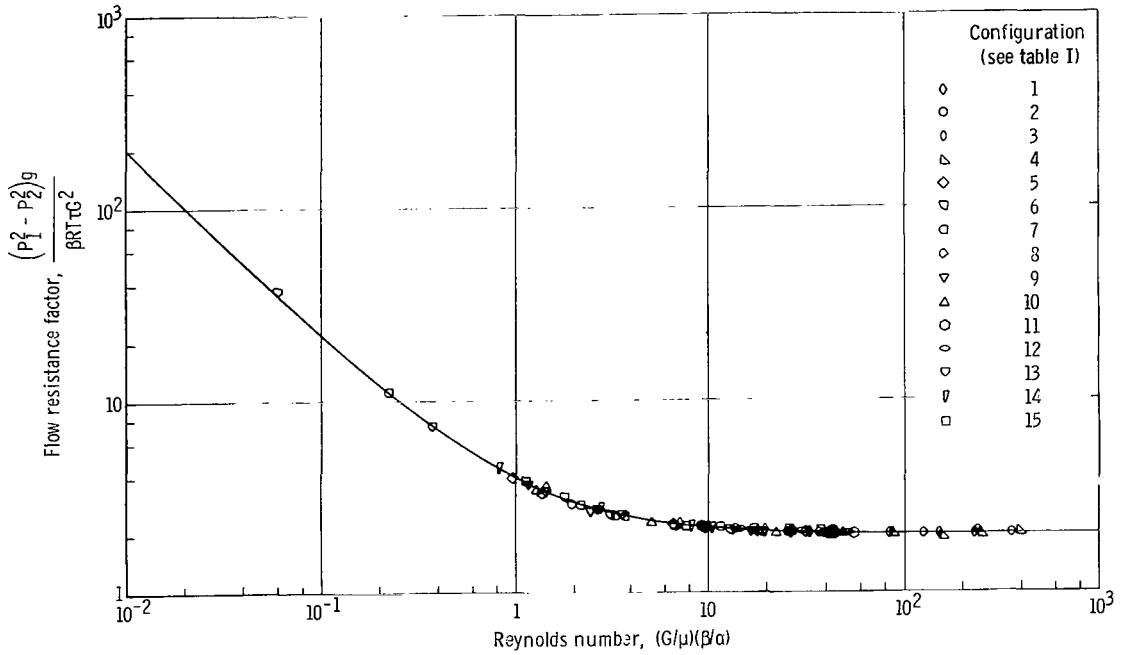


Figure 12. - Permeability correlation data for 15 different Lamilloy configurations.

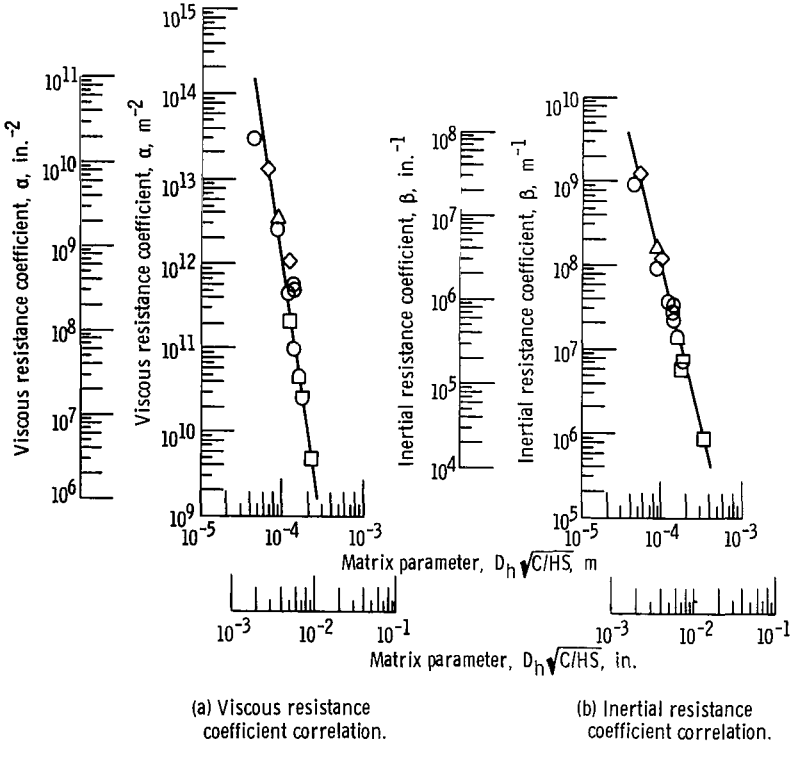


Figure 13. - Flow data correlation for standard array Lamilloy as function of hydraulic diameter and hole spacing. Value of C for viscous and inertial resistance coefficient correlation, 0.244 centimeter (0.096 in.). (From ref. 10.)

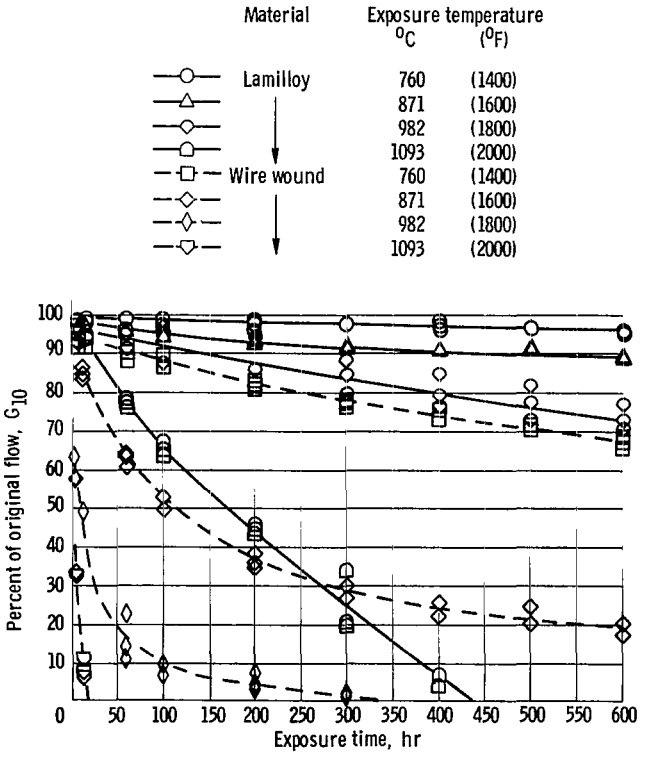


Figure 14. - Change in percent of original flow due to oxidation of disk-type permeability specimens of Lamilloy or wire-wound material made from Hastelloy-X.

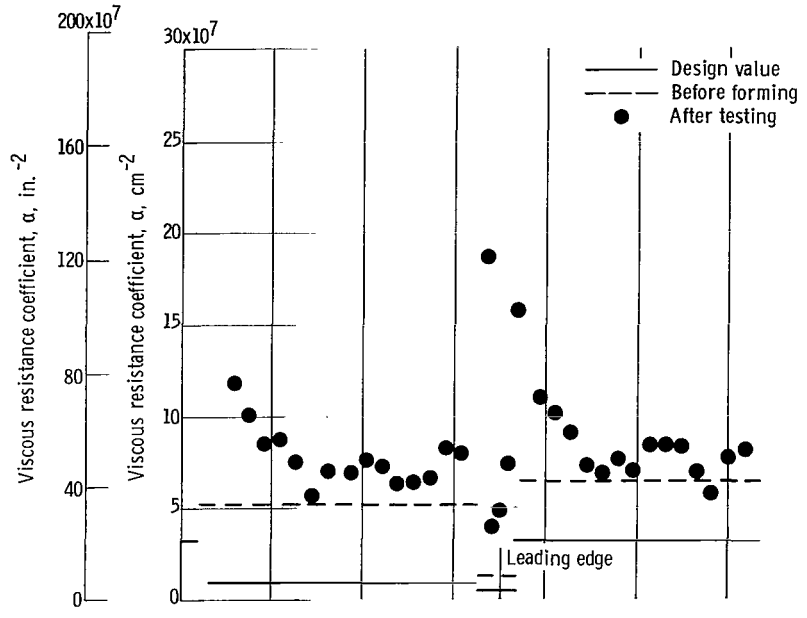


(a) Viscous coefficient, α.

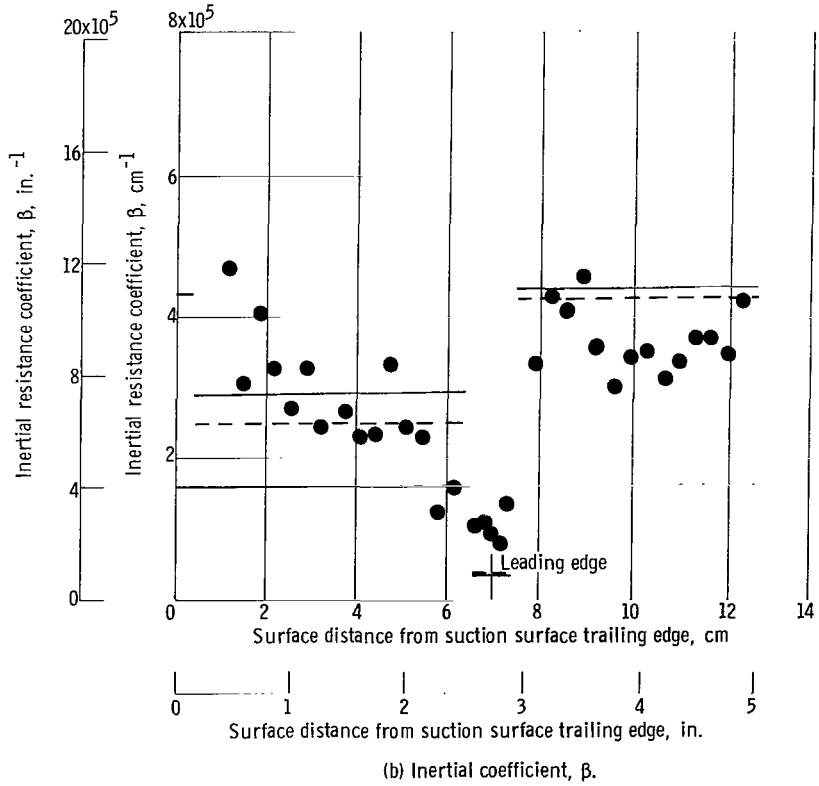


(b) Inertial coefficient, β.

Figure 15. - Typical Lamilloy post-test permeability data for vane midspan.

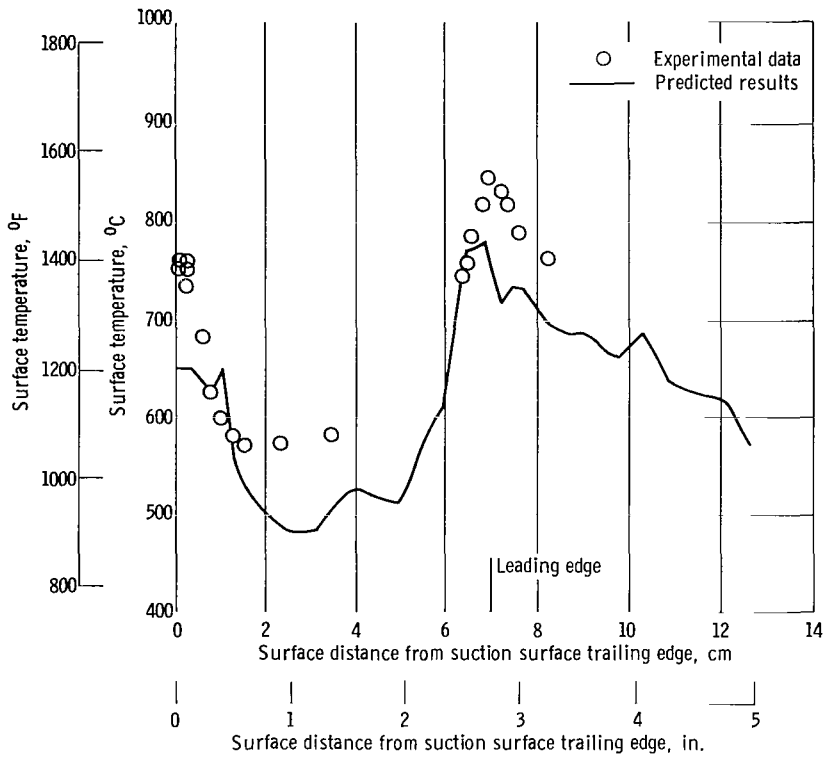


Figure 16. - Comparison of experimental and analytical surface temperatures 3.0 centimeters (1.2 in.) above mean section of Lamilloy vane for nominal gas temperature of 1427° C (2600° F), cooling air temperature of 293° C (560° F), gas stream total pressure of 78.3 N/cm$^2$ (113.5 psi), and ratio of coolant mass flow rate to combustion gas mass flow rate $W_c/W_g$ of 0.0360.

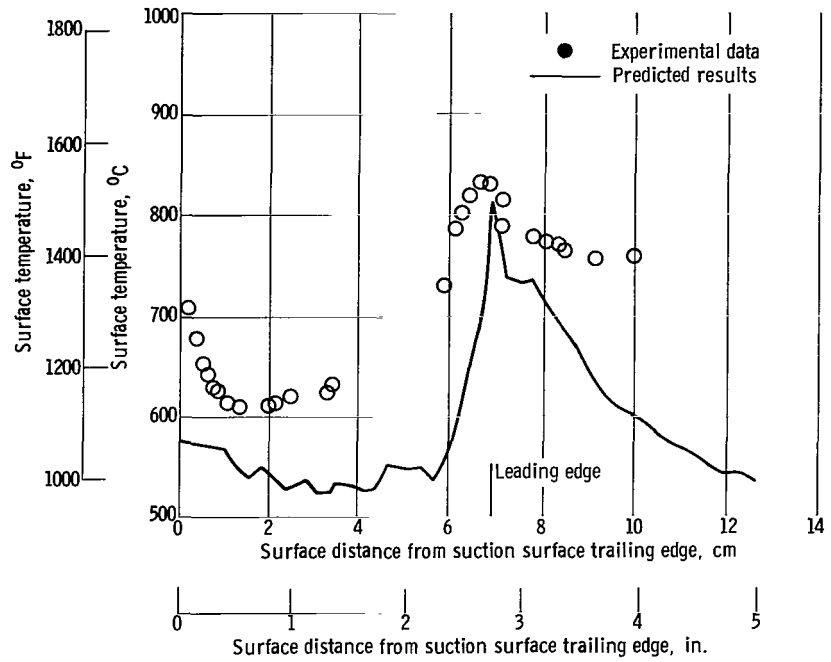


Figure 17. - Comparison of experimental and analytical surface temperatures at mean section of Lamilloy vane for nominal gas temperature of 1388° C (2530° F), cooling air temperature of 293° C (560° F), gas stream total pressure of 97 N/cm$^2$ (140.5 psi), and ratio of coolant mass flow rate to combustion gas mass flow rate $W_c/W_g$ of 0.0376.

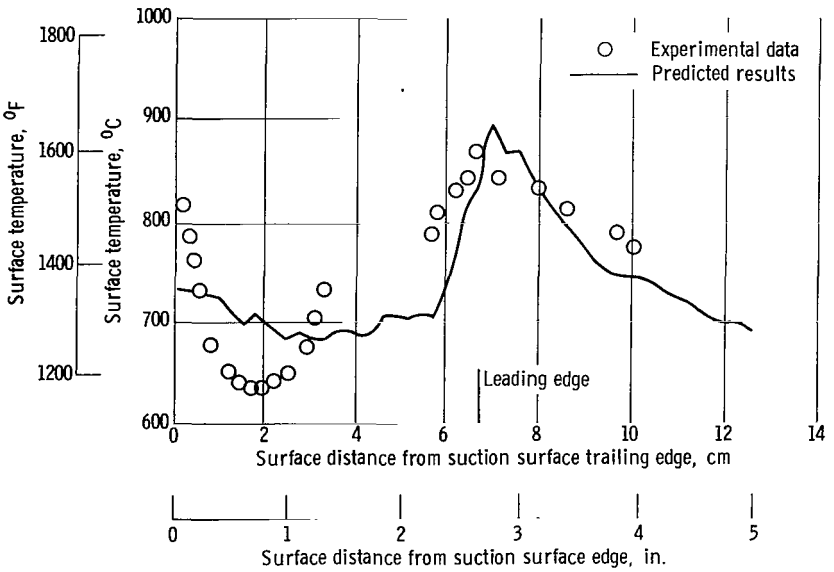


Figure 18. - Comparison of experimental and analytical surface temperatures at mean section of Lamilloy vane for nominal gas temperature of 1399° C (2550° F), cooling air temperature of 454° C (850° F), gas-stream total pressure of 78 N/cm$^2$ (113 psi), and ratio of coolant mass flow rate to combustion gas mass flow rate $W_c/W_g$ of 0.0374.

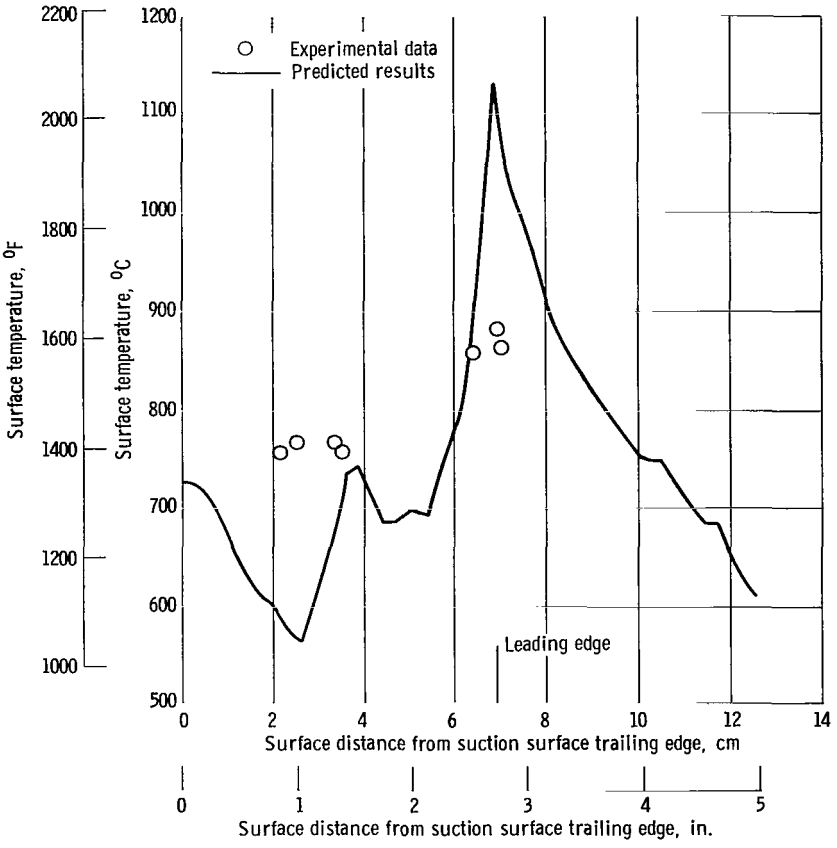


Figure 19. - Comparison of experimental and analytical surface temperatures at 3.0 centimeters (1.2 in.) above mean section of Lamilloy vane for nominal gas temperature of 1741° C (3165° F), cooling air temperature of 316° C (600° F), gas stream total pressure of 79 N/cm$^2$ (114.5 psi), and ratio of coolant flow rate $W_c/W_g$ of 0.0387.

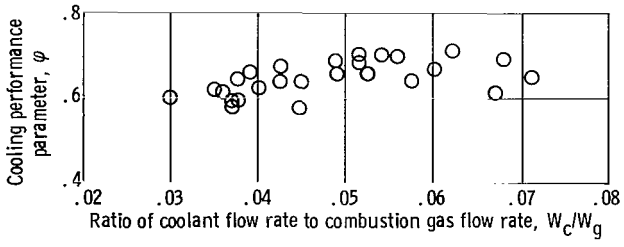


Figure 20. - Effect of cooling air flow rate on cooling performance parameter of Lamilloy vane.

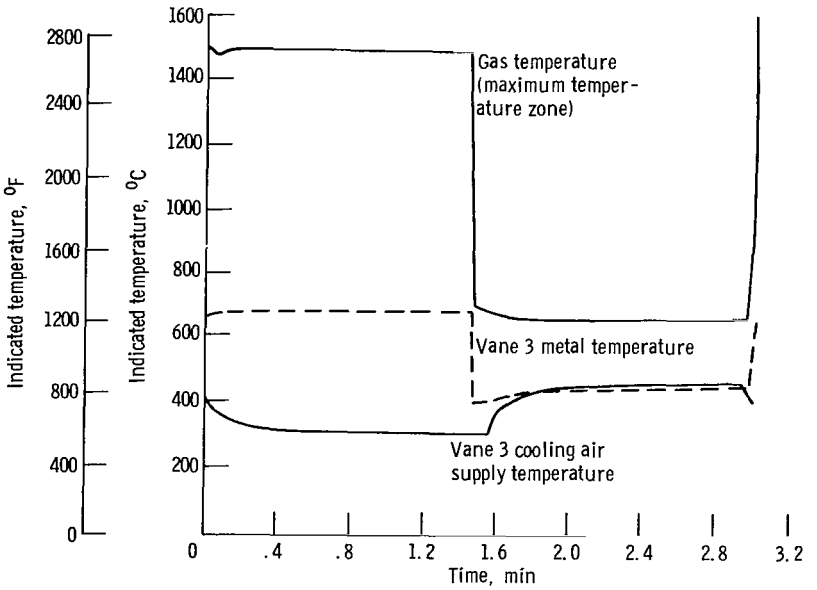


Figure 21. - Cyclic temperature characteristics for Lamilloy vane 3.

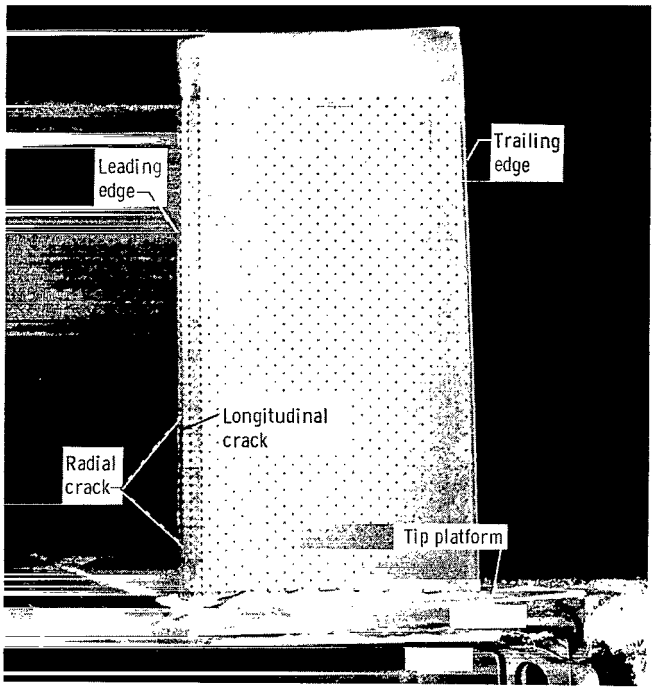


(a) Pressure surface.

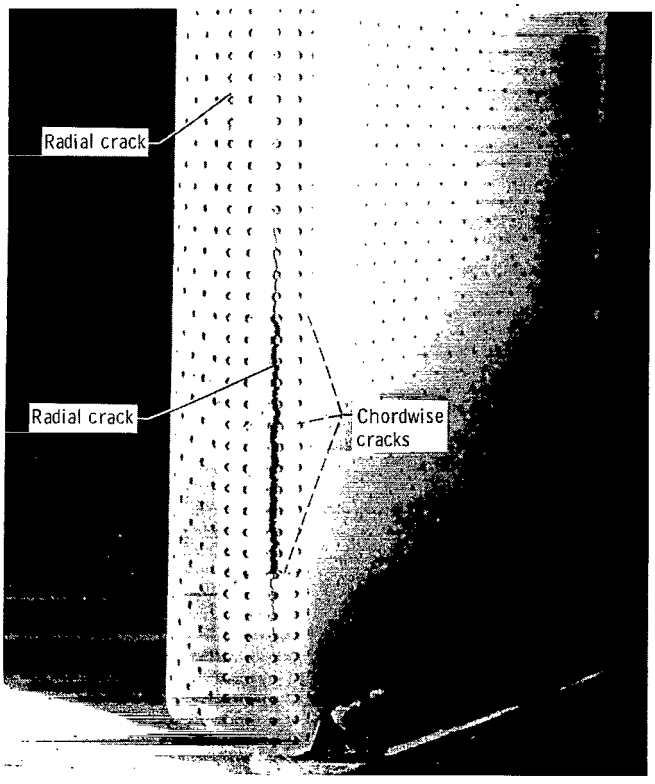


(b) Leading edge.

Figure 22. - Lamilloy vane 2 after 110 thermal cycles.

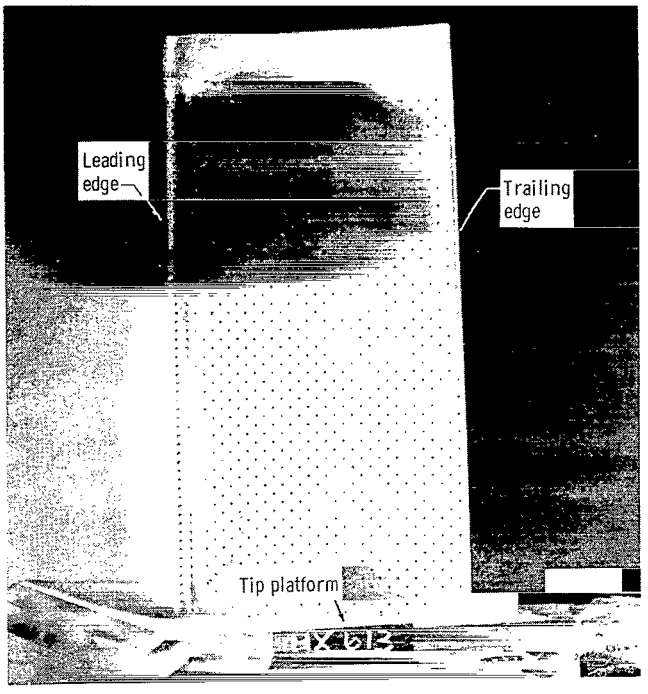


(a) Pressure surface.

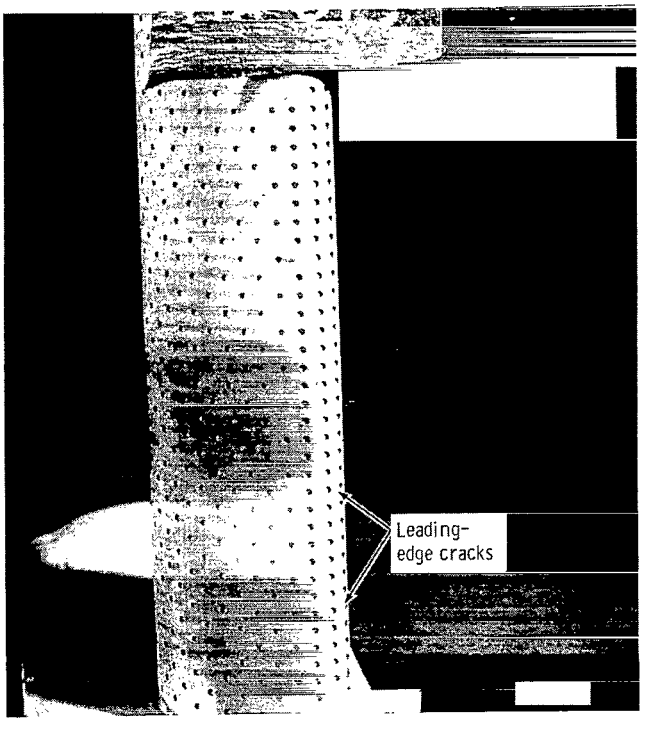


(b) Leading edge and suction surface.

Figure 23. - Lamilloy vane 3 after 110 thermal cycles.

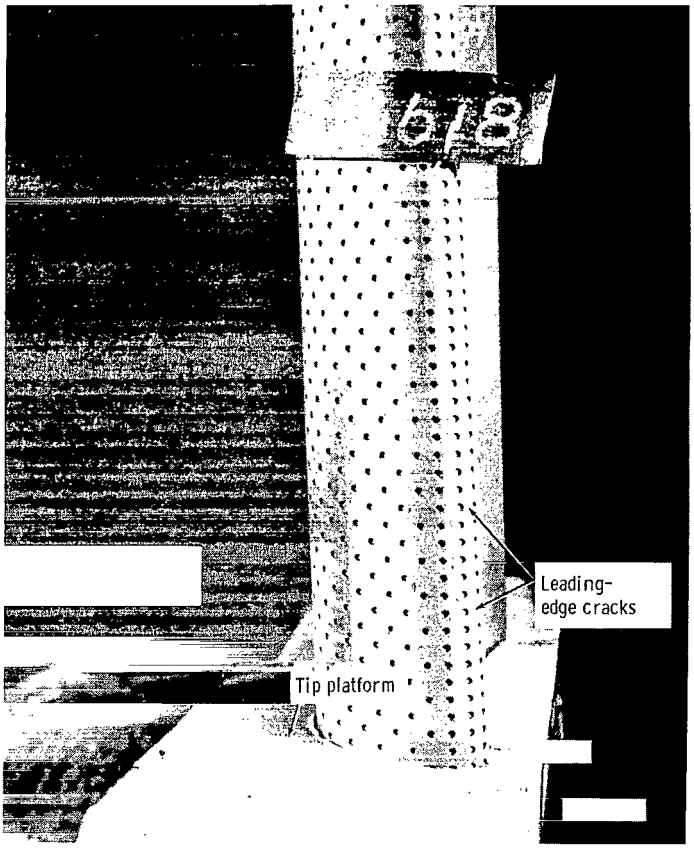


Figure 24. - Leading edge of Lamilloy vane 4 after 110 thermal cycles.

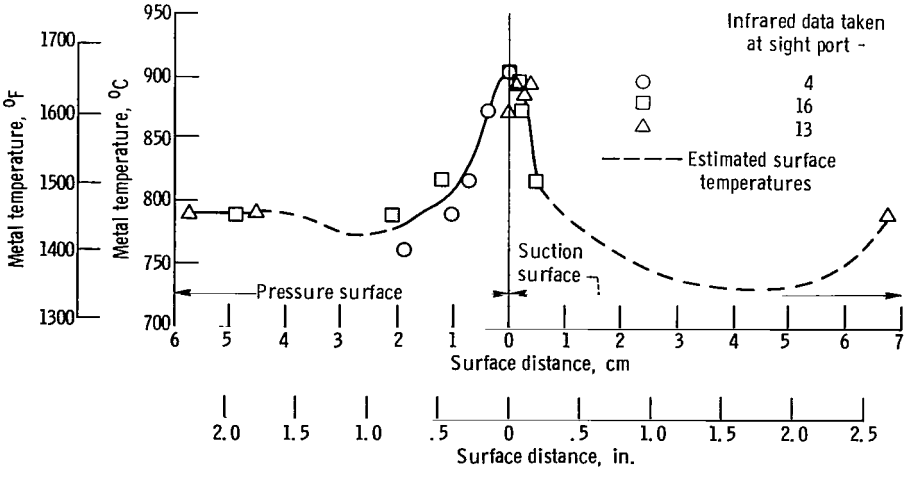


Figure 25. - Measured chordwise temperature distribution at 3/4-span position for Lamilloy vane 2.

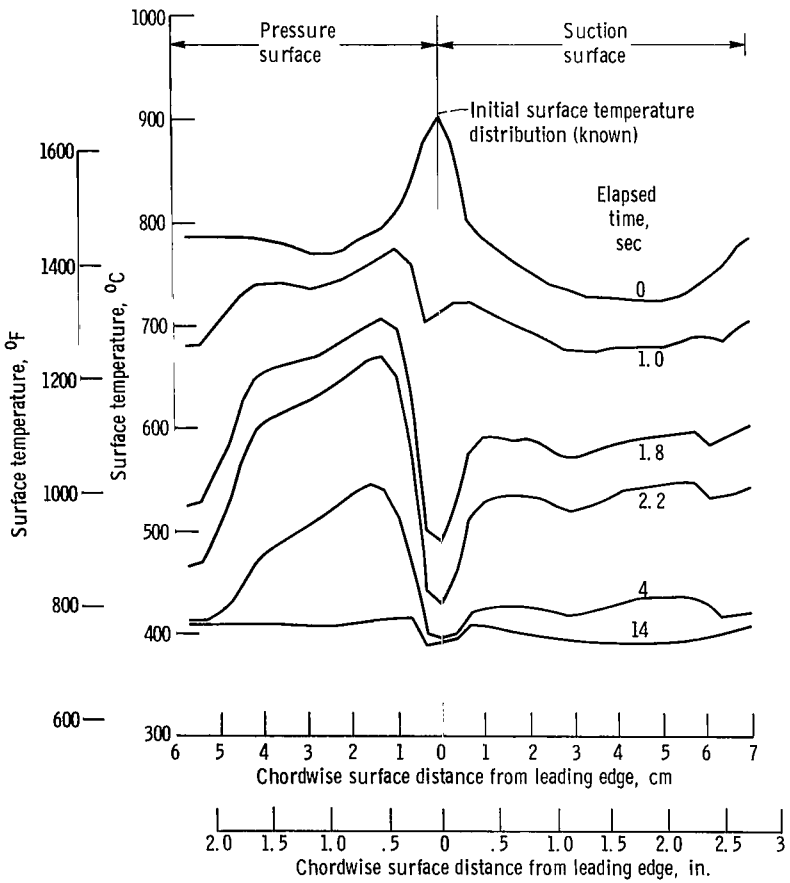


Figure 26. - Predicted transient chordwise surface temperature distribution for Lamilloy vane 2 following a rapid decrease in gas temperature. All results for 3/4-span location.

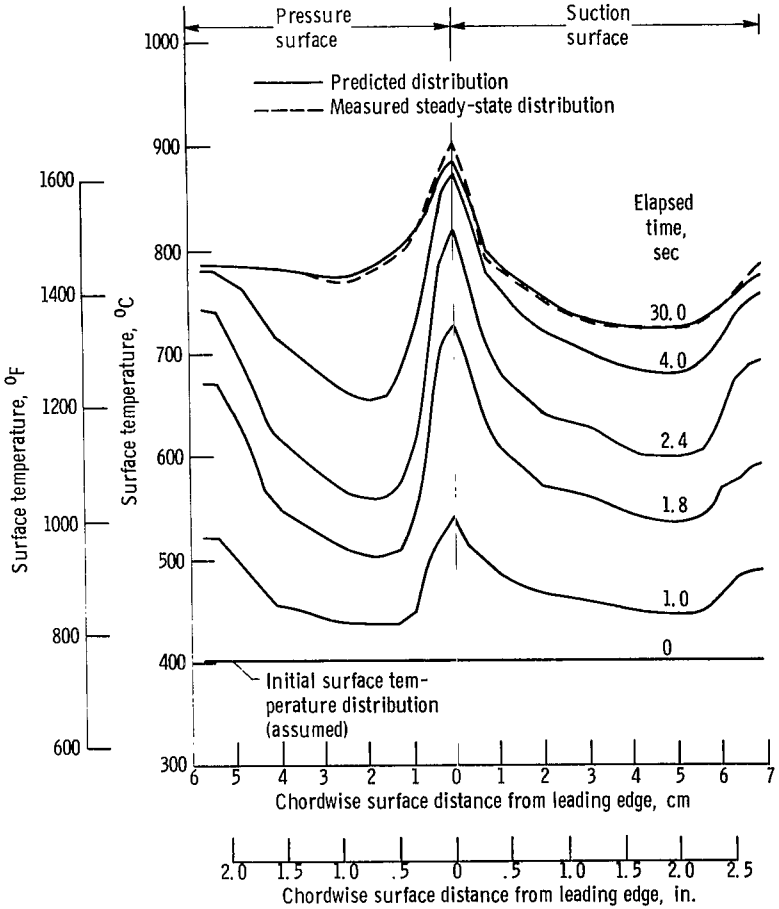


Figure 27. - Predicted transient chordwise surface temperature distribution for Lamilloy vane 2 following a rapid increase in gas temperature. All results for 3/4-span location.

*"The aeronautical and space activities of the United States shall be conducted so as to contribute . . . to the expansion of human knowledge of phenomena in the atmosphere and space. The Administration shall provide for the widest practicable and appropriate dissemination of information concerning its activities and the results thereof."*

—NATIONAL AERONAUTICS AND SPACE ACT OF 1958

# NASA SCIENTIFIC AND TECHNICAL PUBLICATIONS

TECHNICAL REPORTS: Scientific and technical information considered important, complete, and a lasting contribution to existing knowledge.

TECHNICAL NOTES: Information less broad in scope but nevertheless of importance as a contribution to existing knowledge.

TECHNICAL MEMORANDUMS: Information receiving limited distribution because of preliminary data, security classification, or other reasons.

CONTRACTOR REPORTS: Scientific and technical information generated under a NASA contract or grant and considered an important contribution to existing knowledge.

TECHNICAL TRANSLATIONS: Information published in a foreign language considered to merit NASA distribution in English.

SPECIAL PUBLICATIONS: Information derived from or of value to NASA activities. Publications include conference proceedings, monographs, data compilations, handbooks, sourcebooks, and special bibliographies.

TECHNOLOGY UTILIZATION PUBLICATIONS: Information on technology used by NASA that may be of particular interest in commercial and other non-aerospace applications. Publications include Tech Briefs, Technology Utilization Reports and Technology Surveys.

*Details on the availability of these publications may be obtained from:*

**SCIENTIFIC AND TECHNICAL INFORMATION OFFICE**

**NATIONAL AERONAUTICS AND SPACE ADMINISTRATION**

**Washington, D.C. 20546**